MICROCOPY RESOLUTION TEST CHART

NATIONAL BUREAU OF STANDARDS-1963-A

LEVEL

TWINDX: A PLANETARY BOUNDARY LAYER MODEL FOR THE WINDS IN EXTRATROPICAL AND TROPICAL OCEAN AREAS

Prepared By:

Willard J. Pierson
CUNY Institute of Marine and Atmospheric Sciences
The City College of the City University of New York
New York, New York 10031

JUNE 1979

DDC
RECEIVED
SEP 27 1979
E

79 09 26 015

AD A074337

DDC FILE COPY

NEPRF

REPORT DOCUMENTATION PAGE	READ INSTRUCTIONS BEFORE COMPLETING FORM

1. REPORT NUMBER NAVENVPREDRSCHFAC Contractor Report CR-79-02	2. GOVT ACCESSION NO.	3. RECIPIENT'S CATALOG NUMBER

4. TITLE (and Subtitle) TWINDX: A Planetary Boundary Layer Model for the Winds in Extratropical and Tropical Ocean Areas	5. TYPE OF REPORT & PERIOD COVERED Final
	6. PERFORMING ORG. REPORT NUMBER

7. AUTHOR(s) Willard J. Pierson	8. CONTRACT OR GRANT NUMBER(s) N00014-77-C-0206

9. PERFORMING ORGANIZATION NAME AND ADDRESS CUNY Institute of Marine and Atmospheric Sciences The City College of the City University of New York New York, NY 10031	10. PROGRAM ELEMENT, PROJECT, TASK AREA & WORK UNIT NUMBERS PE 62759N PN WF52551792 NEPRF WU 6.2-10

11. CONTROLLING OFFICE NAME AND ADDRESS Naval Air Systems Command Department of the Navy Washington, DC 20361	12. REPORT DATE June 1979
	13. NUMBER OF PAGES 94

14. MONITORING AGENCY NAME & ADDRESS(If different from Controlling Office) Naval Environmental Prediction Research Facility Monterey, CA 93940	15. SECURITY CLASS. (of this report) UNCLASSIFIED
	15a. DECLASSIFICATION/DOWNGRADING SCHEDULE

16. DISTRIBUTION STATEMENT (of this Report)

Approved for public release; distribution unlimited   93p.

17. DISTRIBUTION STATEMENT (of the abstract entered in Block 20, if different from Report)

F52551

18. SUPPLEMENTARY NOTES

Original manuscript dated October 1978   WF52551792

19. KEY WORDS (Continue on reverse side if necessary and identify by block number)

20. ABSTRACT (Continue on reverse side if necessary and identify by block number)

The theory and programming details of a planetary boundary layer model that describes the winds from the surface of the ocean to several hundred meters in the tropics and from the surface to the gradient wind level in extratropical regions are given. The model, called TWINDX for Trade Winds and WINDs EXpanded Scale, is for use on a 123 by 123 polar stereographic projection.

The required input fields are the atmospheric pressure at the sea surface, and the sea surface temperature for the extratropical regions. For the tropical

20. ABSTRACT (Continued)

regions, the sea surface pressure field and field for the height of the lifting condensation level are needed.

Various options are given, and additional options and improvements are described.

The outputs are the vector wind at an elevation of 19.5 meters and the vector wind that would have been measured in a neutrally stratified atmosphere at an elevation of 19.5 meters, along with other fields, as options, that are useful for analysis and interpretation.

The vector wind for a neutral stratification can then be compared with the output of the SASS on SEASAT to remove aliases and provide a wind field that can, in turn, be used to improve on the initial values required for a numerical weather prediction.

Since the preparation of this report, additional material on SEASAT winds and the planetary boundary layer has appeared; a list of supplementary references has been added.

TABLE OF CONTENTS

- ii -

PREFACE

As the finishing touches are being put on this report, it appears that SEASAT has failed in orbit and that no more data will be available from it. The test of these concepts in a real time operational setting to prepare improved weather and wave forecasts is thus not possible at the present time.

Excellent data was obtained with the SASS, the altimeter, and the SMMR for 99 days (a few less for the altimeter). Depending on the mode, there were either about 100,000 or about 200,000 vector winds obtained each day for a total of somewhere between 10 and 20 million vector winds (and their aliases). There are more than enough data and surface truth available to meet nearly all of the objectives of the SASS Experiment Team and to simulate, if desired, some real time applications of the data to determine their impact on forecasts.

1. INTRODUCTION

As designed, the SASS on SEASAT yields from two to four possible
vector winds as candidates for the true wind to be used for specifying
the winds near the surface of the ocean. The theory and computer
programs that have been developed to obtain these vector winds and aliases
have been described in Parts 1 and 2 of this final report. In this
part of the final report, (Part 3), ways to select the true winds,
given the true winds and their aliases from the SASS, by means of an
independent model of the winds based on meteorological field variables
will be described.

The winds near the surface of the ocean are determined at the
synoptic scale from the field of mass of the atmosphere. The details
of the field of mass throughout a substantial layer (500 meters to one
kilometer) of the atmosphere are required, and, in turn, the winds near
the surface of the ocean provide valuable information on the field of
mass for this same layer.

A fundamental feature of the models for winds near the ocean
surface is that they require modern turbulence theory. The variation
of the wind with height between the surface of the ocean and either
the gradient wind level in extra tropical regions or the base of the
cumulus clouds in tropical regions can then be properly described.

There are some aspects of modern turbulence theory that are
presently not universally accepted by the scientific community. A
particularly vexing aspect is that of the relationship between
roughness length and friction velocity so as to define the winds for the
first few meters above the sea surface. Another is the form of
certain non-dimensional functions used in the Monin Obukhoff theory
for the effects of atmospheric stability on the wind profile. Even
deeper lies the problem of the partitioning of the atmospheric

momentum flux into wave generation effects, current production, and dissipation effects. The impact of these uncertainties on the interpretation of the SASS data is considerable because the wind very close to the ocean surface generates the capillary waves that in turn determine most of the backscatter measured by the SASS. In a neutral atmosphere, a synoptic scale average wind at say, 19.5 meters, will produce some stress, some value of u_* and some backscatter versus wind direction and incidence angle relationship. The direct correlation of the 19.5 meter wind with the backscatter avoids specifying a particular relationship for z_o and u_*.

The removal of the SASS aliases will require the use of some boundary layer model over the ocean. Even if the alias problem is eliminated (and it may be in modes 3 and 4 as described in Part 1), the vector winds from the SASS must be used in a way that will influence the analysis of the field of mass or the specification of the initial value conditions in a numerical meteorological forecast.

Plans are already under way to eliminate the alias problem in future oceanic satellites. Nevertheless, a sophisticated model of the winds over the ocean will always be needed for the optimum application of highly accurate remotely sensed vector winds.

Ship reports of the wind speed and direction are among the poorest of the meteorological data conventionally available. These observations are well recognized as being "noisy" - that is, having a large error component. Understandably, with poor data, the various planetary boundary layer models have not had to be very sophisticated so as to "fit" the data with tolerable accuracy.

To further complicate the pre-SEASAT situation, the paucity of ship reports introduces another source of error. The widely scattered reports by ships have to be interpolated and extrapolated over great distances in order to derive the meteorological fields needed to describe the initial state of the atmosphere.

- 2 -

The present state of affairs, that is the pre-SEASAT situation, is indicated in a number of recent studies. One is the S193 report for SKYLAB by Cardone, Young, Pierson, Moore, et al (1976) that showed how poorly conventionally reported winds specified the winds for the SKYLAB program. Another is the study by Pierson and Salfi (1978) that showed that the major source of error in the SOWM forecasts was probably the winds that drove the model. The last is the report, based on research at the Goddard Space Flight Center, given by Cardone to the National Ocean Satellite System User Working Group on July 20, 1978, which showed that simulated SEASAT data would be capable of correcting erroneous wind fields with errors of 3 M/S to 6 M/S over the North Pacific.[†]

In the SEASAT era, the winds over the ocean will become the most accurately and most densely observed quantity over the ocean. When the information that they provide is properly incorporated into the analysis of the planetary boundary layer over the oceans, the improved specification of the various meteorological fields that result will have a direct impact on improved meterological forecasts.

2. THE NATURE OF THE SASS WINDS

For scanning mode 1,[*] (vertical polarization all beams), the output of a SASS wind vector algorithm will be from two to four vector winds for each pair of close-by cells in the two swaths. It is assumed that the "Model Function" has been correctly defined. For moderate and high winds, and for incident angles near 40°, it is expected that the errors in the vector winds (once the aliases are removed and corrections for attenuation are applied) will be about $\pm$ 0.5 M/S and $\pm 5^{o}$ to 10°, if the wind is not too close to upwind or downwind for one of the beams. Moreover there will be sixteen, or so, winds near a given point of a numerical model, and vector avera-

---

[†] See Cane, Cardone, Halem et al. (1978).

[*] And all other modes except 3 and 4.

ging should yield errors of about $\pm$ 0.12 M/S and $\pm$ 1.25° to 2.5°. Near
upwind or downwind, there will be a tendency to "lock on" the upwind
and downwind values. The speeds will be very accurate, and a wider
range of direction errors will occur. Typical uncertainties in the
winds and typical patterns for the directions and speeds of the "true"
and aliased winds are shown in both Appendix B and Appendix C of
this final report. When four winds are recovered, they can be as
much as 90° apart and as little as 15° or 20° apart.

Once the model function is perfected, there will be numerous
points for which one of the two recovered winds will have a very
high probability of being the correct wind and that will have a narrow
range for direction and speed errors. At other points, a decision
will have to be made between two wind vectors that are 180° apart
in direction. At still other points in the same field, there will
be three vector winds, forming a "Y" pattern with the base of the
"Y" at either upwind or downwind.

3. SURFACE WINDS, THE ATMOSPHERIC FIELD OF MASS, AND TURBULENCE

Efforts to relate the surface winds and the atmospheric field
of mass are as old as the science of synoptic meteorology. Given
a single wind speed and direction, ways to use that information have
been the subject of study for many decades, going back to a meteoro-
logical law, first proposed by William Ferrel, which stated that
high pressure would be at the right if a person stood with his
back to the wind in the northern hemisphere. This meteorological
law is usually attributed to Christopher Hendrik Didericus Buys Ballot
who also stated it in 1854. It has become known as Buys Ballot's Law.

Although stated, the relationshop was not particulaly quantitative as in Brunt (1942), Brunt (1944) and Petterssen (1940). Minor modifications such as a 30° correction, or so, toward low pressure over the oceans were quickly made, and it was recognized that the law did not work well in the tropics.

Since isobars could "easily" be drawn into areas where there were no ship reports, there followed efforts to calculate the winds near the surface of the ocean by means of empirical corrections to the gradient and geostrophic vector winds calculated from the isobaric pattern. Johnson (1955) was an early effort to do this, in which air-sea temperatures differences were shown to have an effect on the ratio of the sea surface wind to the geostrophic wind.

The need to relate the surface winds over the ocean to synoptic meteorological fields resulted in a study by Thomasell and Welsh (1963), which was an effort to improve on the specification of the winds for numerical wave specification and forecasting as illustrated by the work of Baer (1962). Multiple regression techniques were developed that predicted the surface wind as reported by both weather ships and transient ships. Many different variables were used to predict the wind such as the gradient and geostrophic winds, the air-sea temperature difference, the gradient of the 1000 mb to 700 mb thickness and various vorticity fields. About 55% of the variance of the magnitude of the wind, as reported by both weather ships and transient ships, could be specified, and only 5% of the variability in direction could be accounted for. The error in specifying the direction was 35°. The mean inflow angle (or cross isobar angle) was 15.5°.

In retrospect, this research was only partially on the right track. The physics of the planetary boundary layer did not enter into the model equations in a satisfactory way. As examples, the 1000 to 700 mb thickness is too great to allow the proper treatment of thermal wind

effects, and the air sea temperature difference has subtle effects that
cannot be modeled as a linear term. Moreover, the other half of the
problem, namely the accuracy of the wind speed and direction as reported
by the ships was not considered as a source of the differences between
the values specified by the regression equations and the values reported
by the ships.

A problem of the time was that of the value of what is now called
the Charnock constant, (See Mellville (1977)) say, α_c, in the non-
dimensional relationship given by equation (1) for ocean wave heights.

$$\frac{gH}{v^2} = \alpha_c \qquad (1)$$

Charnock (1955) pointed out that this constant varied by a factor of
about two, depending on the source. Pierson (1964) noticed that one of the
major sources for the differences in the value of α_c was that the winds used
in (1) had been referred to different anemometer heights varying from 7.5
to 19.5 meters. The differences in wind speeds at these different
heights, as calculated for various drag coefficients, explained a major
part, but not all, of the differences between the various values of
the Charnock constant. The important point though, with reference to the
measurement and specification of the winds over the ocean, is that varia-
tions in the anemometer height need to be calibrated out in any effort
to compare winds reported by ships to winds specified from meteorological
fields. Variations in anemometer height were one of the sources of
the residual unexplained variance in the study by Thomasell and Welsh (1963).

4. THE OCEANIC BOUNDARY LAYER MODEL OF CARDONE

A continued effort to improve on the specification of the winds near the surface of the ocean for wave forecasting purposes lead to an oceanic boundary layer model developed by Cardone (1969). Because of the absence of strong diurnal heating effects over the ocean, the specification of the winds for the first kilometer above the ocean surface is somewhat simpler than the corresponding problem over land.

The boundary layer model of Cardone (1969) was used in the development of the spectral ocean wave model (SOWM) described by Salfi (1974) and Lazanoff and Stevenson (1975). It applies to extratropical regions and is not expected to provide useful results close to the equator. Also strong inversions in the first kilometer above the surface do not coincide with the assumptions of the model.

The model developed for SEASAT is essentially this boundary layer model of Cardone extended to a 123 by 123 grid, instead of a 63 X 63 grid, on a polar stereographic projection. It has been modified for tropical areas on the basis of a note prepared by V. Wong and T.N. Krishnamurti (1978). Tests of the 63 X 63 grid showed poor resolution of synoptic scale features so that the 123 by 123 grid becomes an important extension.

The boundary layer model that results from combining the Cardone model for the extratropical regions and the Wong and Krishnamurti results for the tropical regions on a 123 by 123 grid will be referrred to as TWINDX, for trade winds and winds, expanded scale. The initial programs developed for these models start with the work of Thomasell and Welsh (1963). The technical details of the computer program will be given first, and then the theories involved in the two boundary layer models will be summarized. The programs still have to be modified for the southern hemisphere.

- 7 -

5. PROGRAM TWINDX

5.1 Inputs

The inputs to PROGRAM TWINDX (TRADE WINDS AND WINDS EXPANDED) are
four fields for the ocean points of a 123 by 123 FNWC polar stereographic
grid. The fields are sea surface pressure in millibars, air temperature
in degrees Celsius at 10 meters above the sea surface, sea surface tempera-
ture in degrees Celsius and the height of the lifting condensation level.
Pressures and temperatures over nearby land are also needed so that gradiants
near ocean points can be found.

5.2 Outputs

The outputs are the synoptic scale average wind speed in m/s and wind
direction in degrees (meteorological convention) at each ocean grid point
at an elevation of 19.5 meters above the sea surface. Both the actual
wind and the equivalent wind for a neutrally stratified atmosphere can
be obtained. The equivalent wind for a neutrally stratified atmosphere
is the value obtained by SEASAT.

5.3 Supplementary Outputs

Additional outputs for analysis purposes can be the direction and
speed of the gradient wind in extratropical regions; the vector wind
stress at the sea surface for any one of three z_o versus n_* relationships, the
friction velocity,* the Monin-Obukhoff length, and the height of the
constant flux layer. In the tropics, the wind from the top of the log-
arithmic profile layer to the cloud base can be obtained.

5.4 Constraints and Options

Any one of three roughness length versus friction velocity relation-
ships can be used. The Cardone-low, Garratt high relationship is
recommended.

For extratropical areas, the geostrophic wind is calculated from
the surface isobaric field. This wind is corrected for isobaric

---

* as a vector

curvature to obtain the gradient wind. Bounds are placed on the deter-
mination of the gradient wind so that it is not less than 0.7 times
the geostrophic wind for cyclonically curved isobars and not greater
than 1.3 times the geostrophic wind for anticyclonically curved isobars.
These bounds can be changed by changing two lines of code in the program.

The curvature of the isobars can be calculated either from the
spacings of the 123 by 123 grid or from points twice as far away (to
smooth the calculation) by setting KV equal to either one or two.

For light winds in extratropical regions, 0.7 times the geostrophic
wind has been used, and the wind direction has been turned 15° toward
low pressure. The variation with height of the geostrophic wind is
found from the air temperature field so as to account for thermal
wind effects.

Below the height, h, the wind direction is constant with height and
is defined by the Monin-Obukhoff theory, which requires information on
the air-sea temperature difference, so as to determine the Monin-
Obukhoff stability length where

$L > 0$ stable $(\theta_a > \theta_s)$, θ_a not greater than $4^{\circ}c + \theta_s$

$L < 0$ unstable $(\theta_a < \theta_s)$

$L = \infty$ neutral (infinite is listed as zero)

An internal boundary condition is satisfied at the height, h, such
that the eddy viscosity is constant above h and an Ekman spiral plus the
thermal wind define the wind and such that below, h, the Monin-
Obukhoff wind profile applies in the constant flux layer. The internal
boundary conditions are that wind speed and direction are continuous at
h and that the wind shear is continuous at h. The height, h, is checked
to be sure that it is always greater than or equal to 19.5 meters.

The tropical model assumes a logarithmic profile below 35 meters
and a constant wind speed and direction to the lifting condensation
level. The balance of forces that is used are for the atmospheric

layer between 35m and the lifting condensation level. This balance is between the pressure gradient acceleration and the coriolis acceleration and a term involving the wind stress, <u'w'>, and the thickness of the layer from 35 m to the LCL. Vector wind fields are continuous at the equator.

The choice of points for which the tropical model is used is as follows. All points equatorward of 20°N and 20°S use the tropical model. If the wind has a component toward the equator, and if the LCL is known, and if the grid point is between 30°N and 20°S, the tropical model is used. Minor changes in the program can extend or decrease the area for the tropical analysis. In an earlier version, without the tropical portion, the coriolis term equatorward of 10°N (or S) was set equal to the value at 10° and the winds were computed using the Cardone boundary layer theory.

6. THEORY OF THE EXTRATROPICAL BOUNDARY LAYER

6.1 Ekman

The governing diagnostic equations for the time averaged horizontal synoptic scale winds above some height, h, and up to the gradient wind level are given by equations (2) and (3).

$$\bar{u}_t + \bar{u}\bar{u}_x + \bar{v}\bar{u}_y - f\bar{v} = -\bar{p}_x/\rho + K_M \bar{u}_{zz} \tag{2}$$

$$\bar{v}_t + \bar{u}\bar{v}_x + \bar{v}\bar{v}_u + f\bar{u} = -\bar{p}_y/\rho + K_M \bar{v}_{zz} \tag{3}$$

For $\bar{P}_x$ and $\bar{P}_y$ constant with height and no local isobaric curvature so that the geostrophic wind is constant with height, and for the boundary condition that

---

* Momentum flux through the cloud base is also needed in principle, but it has been assumed to be zero.

$$\vec{V} = \vec{V}_{Geostrophic} \qquad (4)$$

at infinity and

$$\vec{V} = 0 \qquad (5)$$

at the surface (which is not actually used), and for non accelerated motion (i.e. $\bar{u}_t = \bar{v}_t = 0$), the solution is the well known Ekman spiral, referred to a coordinate system where $\bar{P}_x$ is zero as in equation (6).

$$u = V_G (1 - e^{-a h} \cos \bar{a}h) \qquad (6a)$$

$$v = V_G e^{-a h} \sin a h \qquad (6b)$$

where

$$V_G = \frac{1}{\rho f} \partial \bar{p} / \partial y \qquad (7)$$

and

$$a = (f/2 \ K_M)^{\frac{1}{2}} \qquad (8)$$

The Ekman spiral is unrealistic near the ocean surface because K_M cannot be treated as a constant.

In TWINDX, the gradient wind is calculated and used to replace the geostrophic wind, but the shape of the Ekman spiral is not corrected for the effect of the curved isobars.

For anticyclonic curvature,

$$\vec{V}_{GR} > \vec{V}_{GEO} \qquad (9)$$

- 11 -

and conversely for cyclonic curvature

$$\vec{V}_{GR} < \vec{V}_{GEO} \tag{10}$$

Bounds are placed on the gradient wind so that it lies within 0.7 to 1.3 times the geostrophic wind.

The curvature of the sea surface isobars is used to convert from the geostrophic wind to the gradient wind. It is calculated from the finite difference version of equation (11), and as such involves the second differences of pressures at a given point in the field and the eight surrounding points.

$$K = \frac{\frac{\partial^2 p}{\partial x^2}\left(\frac{\partial p}{\partial y}\right)^2 + \frac{\partial^2 p}{\partial y^2}\left(\frac{\partial p}{\partial x}\right) - \frac{1}{2}\frac{\partial^2 p}{\partial x \partial y} \cdot \frac{\partial p}{\partial x}\frac{\partial p}{\partial y}}{\left(\left(\frac{\partial p}{\partial x}\right)^2 + \left(\frac{\partial p}{\partial y}\right)^2\right)^{\frac{3}{2}}} \tag{11}$$

In (11), the sign of K accounts for cyclonic or anticyclonic curvature.

This particular finite difference computation can produce erratic values for the factor that multiplies the geostrophic wind to generate the gradient wind, and so an option is provided that permits using grid points that are twice as far apart for this finite difference calculation.

The gradient wind is calculated from the geostrophic wind by means of equation (12), where r = 1/K.

$$\frac{V_{GR}^2}{fr} + V_{GR} = V_{GEO} \tag{12}$$

6.2 The Variation of the Gradient Wind With Height

In general, $\bar{P}_x$ and $\bar{P}_y$ are not constant with height from the surface to the gradient wind level. At each elevation, z, above the surface, the geostrophic wind has a different speed and direction. If the rate of change with height of the geostrophic wind is constant throughout the boundary layer above the height, h, it is possible to write equation (13) in which $(z-h)(\vec{dG}/dz)$ would be the thermal wind vector at z. The quantity, $\vec{dG}/dz$, is treated as a constant.

$$\vec{V}_{Total}(t) = \vec{V}_{Ekman} + z\left(\frac{d\vec{G}}{dz}\right) - h\left(\frac{d\vec{G}}{dx}\right) \tag{13}$$

The quantity, $\left|\vec{dG}/dz\right|$, can be calculated from the horizontal gradient of the input air temperature field, at 10 meters above the sea surface, where the magnitude of the vector is given by (14). One of the disadvantages of the model is that it requires the air temperature as an input and that air temperature is presently not a remotely sensed quantity. The direction of $\vec{dG}/dz$ lies parallel to the surface isotherms and high temperature is on the right.

$$f\left|\frac{d\vec{G}}{dz}\right| = f\left|\frac{dV_{GEO}}{dz}\right| = g\frac{dT/dn}{T} \tag{14}$$

An important feature of equation (13) is that equation (15) still holds so that the Ekman solution for equations (2) and (3) is still valid at and above h.

$$\frac{\partial^2 \vec{V}_{Total}}{\partial z^2} = \frac{\partial^2 \vec{V}_{Ekman}}{\partial z^2} \tag{15}$$

6.3 The height, h

The vector wind is thus defined as the sum of an Ekman Spiral[*] and the appropriate portion of the thermal wind at each elevation, z, above the height, h. This height is defined by equation (16) if h > 19.5 meters and by h = 19.5 meters if (16) yields a value less than 19.5 meters when the wind is light.

$$h = B_o \, | \vec{V}_{GR} | \, / \, f = 3 \times 10^{-4} | \vec{V}_{GR} | \, / \, f \qquad (16)$$

6.4 The Monin-Obukhoff Similarity Theory for the Surface Boundary Layer

Below the height, h, the eddy viscosity is no longer a constant and is defined as K_u instead of K_M. Horizontal pressure gradients and the various other terms in the equations of motion are all relatively unimportant. The wind does not change direction with height and is a function of height only as in equation (17) in which the wind vector direction is the mean wind direction.

$$\bar{u} = \bar{u} \, (z) \qquad (17)$$

The governing equation is the requirement that the eddy flux of momentum is constant with height as in equation (18).

$$\frac{\partial}{\partial z} < w' \, u' > \, = 0 \qquad (18)$$

---

[*] The Ekman spiral that results is not the one from (6a) and (6b) as will be shown later.

- 14 -

This implies that

$$- < w'u' > = K_u \frac{d\bar{u}}{dz} = u_*^2 = \tau/\rho \qquad (19)$$

and that

$$\frac{\partial}{\partial z} u_*^2 = 0 \qquad (20)$$

so that the layer from the surface to h is a constant stress layer.

The eddy viscosity in this layer increases linearly with height and can be defined in terms of a mixing length as in equation (21) where $\kappa = 0.41$ for this model

$$K_u = u_* \ell = \kappa u_* z \qquad (21)$$

From equation (19) and from

$$K_u \frac{\partial \bar{u}}{\partial z} = u_*^2 \qquad (22)$$

it follows that

$$u_* = \kappa z \, d \, \bar{u}/dz \qquad (23)$$

or that

$$\frac{\partial \bar{u}}{\partial z} = \frac{u_*}{\kappa z} \qquad (24)$$

For a neutrally stratified atmosphere, this equation integrates to the logarithmic wind profile as given by equation (25).

$$\bar{u}(z) - \bar{u}(z_o) = \frac{u_*}{\kappa} \ell n \, (z/z_o) \qquad (25)$$

- 15 -

If z_o were known, the wind speed would be given as a function of height above the sea surface. $u(z_o)$ is usually set equal to zero.

For a non-neutrally statified atmosphere, the Monin-Obukhoff (1954) similarity theory is applied in terms of the non-dimensional wind and temperature profiles above the sea surface. The requirement is that the flux of heat be constant as in equation (26).

$$< w'\theta' > = H = Q/\rho \, C_p \qquad (26)$$

A non-dimensional length scale, $\zeta = z/L$ is used in which L is the Monin-Obukhoff stability length defined by

$$L = \frac{< w'u' >^{u_* \, T_o}}{< w'\theta' > \, \kappa \, g} \qquad (27)$$

The fluxes are given by equation (28) and (29) (Tchen (1977)).

$$- < w'u' > = K_u \, d \, \bar{u} \, / \, d \, z \qquad (28)$$

$$- < w'\theta' > = K_\theta \, d \, \bar{T} \, / \, d \, z \qquad (29)$$

By means of the mixing length hypothesis

$$K_u = \kappa \, u_* \, z \left[\varphi_u \, (\zeta) \right]^{-1} \qquad (30)$$

$$K_\theta = \kappa \, u_* \, z \left[\varphi_\theta \, (\zeta) \right]^{-1} \qquad (31)$$

and the Prandtl Number, say, λ is then

$$\lambda = \frac{K_\theta}{K_u} = \frac{\varphi_u}{\varphi_\theta} \cong 1 \qquad (32)$$

which is assumed to be nearly equal to one.

- 16 -

The nondimensional wind shear and temperature gradient are then given by equations (33) and (34) where T_* is given by (35).

$$\frac{\kappa z}{u_*} \frac{\partial \bar{u}}{\partial z} = \varphi_u(\zeta) \tag{33}$$

$$\frac{\kappa z}{T_*} \frac{d\bar{T}}{dz} = \varphi_\theta(\zeta) \simeq \varphi_u(\zeta) \tag{34}$$

$$T_* = -\frac{<w'\theta'>}{u_*} = H/u_* \tag{35}$$

For the variation of wind with height between the surface and $z = h$, the problems then become those of finding the value of L, the functional form for $\varphi_u(\zeta)$ and of integrating equation (28).

Formally, the solutions are given by (36) and (37) where it should be noted that (37) can be rewritten as (38).

$$\bar{u}(z) = \frac{u_*}{\kappa} (\ell n(z/z_o) - \Psi(z/L')) \tag{36}$$

$$L' = \frac{u_*^2 \bar{\theta} (\ell n(z_a/z_o) - \Psi(z_a/L'))}{\kappa^2 g (\theta_a - \theta_s)} \tag{37}$$

$$L' = \frac{u_*}{\kappa} \frac{\bar{u}(a) \bar{\theta}}{g(\theta_a - \theta_s)} \tag{38}$$

For (37) and (38), the wind speed has to be evaluated at 10 meters, which is assumed to be the elevation above the sea surface at which the air temperature is measured. The quantity, L', is an estimate of L (equation 25) in bulk aerodynamic form in terms of quantities that can be measured on a ship, with the exception of u_*. If the air temperature, θ_a, is greater than the sea surface temperature, θ_s, L' is greater than zero (the stable case). If $\theta_a < \theta_s$, L' is less than zero (the unstable case). For $\theta_a = \theta_s$, L' is infinite and equation (33)

- 17 -

is used (the neutral case).

Equation (33) can formally be integrated as follows in (39).

$$\bar{u}(z) = \frac{u_*}{K} \int_{z_0}^{z} \frac{\varphi_u \ (z'/L')}{z'} \ d \ z'$$ (39)

However it is more instructive to define

$$\Psi \left(\frac{z}{L'}\right) = \int_{z_0/L'}^{z/L'} \left[\left(1 - \varphi(\zeta)\right)/\zeta\right] d \ \zeta$$ (40)

and to note that the derivative of (36) is

$$\frac{d\bar{u}}{dz} = \frac{u_*}{K} \left(\frac{1}{z} - \frac{\partial \Psi}{\partial z}\right)$$ (41)

and that from (40)

$$\frac{\partial \Psi}{\partial z} = \frac{\left[1 - \varphi(z/L')\right]}{(L') \ (z/L')}$$ (42)

so that

$$\frac{\partial \bar{u}}{\partial z} = \frac{u_*}{K} \left[\frac{1}{z} - \left(\frac{1}{z} - \frac{\varphi(z/L')}{z}\right)\right] = \frac{u_*}{K} \frac{\varphi(z/L')}{z}$$ (43)

- 18 -

The nondimensional wind shear, $\varphi_u(z/L')$, has to be determined from experiment. There have been many different functions of $x/L' = \zeta$ proposed. A few of them for an unstable atmosphere are given below along with the source (from Tchen (1977) and Meresca (1977)).

$$\varphi_u = (1 - 15\zeta)^{-\frac{1}{4}} \tag{44a}$$

$$\varphi_\theta = 0.74 (1 - 9\zeta)^{-\frac{1}{2}} \tag{44b}$$

from Dyer and Hicks (1970)

$$\varphi_u = (1 - 16\zeta)^{-\frac{1}{4}} \tag{45}$$

from Panofsky and Peterson (1972)

$$\varphi_u = (1 - 15\zeta)^{-\frac{1}{4}} \tag{46a}$$

$$\varphi_\theta = (1 - 15\zeta)^{-\frac{1}{2}} \tag{46b}$$

from Businger et al. (1971).

For a stable atmosphere,

$$\varphi_u(\zeta) = 1 + \beta' \zeta \tag{47}$$

with β' variously given as 5 or 7.

The form actually used in TWINDX is the one proposed by Panofsky (1963), the so-called KEYPs formulation, for unstable conditions and $\beta' = 7$ for stable conditions.

For stable conditions, from equation (40),

$$\Psi\left(\frac{z}{L'}\right) = -\int_{z_o/L'}^{z/L'} \beta' \, d'\zeta = \beta' \, z/L' \qquad (48)$$

so that

$$\bar{u}\,(z) = \frac{u_*}{\kappa}\left(\ln \frac{z}{z_o} + \frac{\beta' z}{L'}\right) \qquad (49)$$

The KEYPS relationship is given by equation (50).

$$\varphi_u^4 - 18 \, (z/L') \, \varphi_u^3 - 1 = 0 \qquad (50)$$

It is necessary to express φ_u as a function of z/L' and to evaluate equation (40) in order to find $\Psi(z/L')$. This is accomplished by defining an auxiliary parametric variable R_i (a Richardson number) such that both z/L' and φ_u are functions of R_i. Then as R_i is varied, the pairs of values of z/L' and φ_u that result define φ_u as a function of z/L'. This Richardson number is defined by equation (51).

$$R_i = \frac{g}{\theta} \frac{(d\theta/dz)}{(du/dz)^2} = \frac{z}{L'} \frac{1}{\varphi_u(z/L')} \qquad (51)$$

From (51),

$$\varphi_u = \frac{z}{L'} \frac{1}{R_i} \qquad (52)$$

- 20 -

and (52) can be substituted into (50) to obtain

$$\left(\frac{z}{L'}\right)^4 \frac{1}{(\Re_i)^4} - 18\left(\frac{z}{L'}\right)^4 \frac{1}{(\Re_i)^3} - 1 = 0 \tag{53}$$

From (53), the result is that z/L' can be expressed in terms of $\Re_i$ as equation (54).

$$\frac{z}{L'} = \Re_i \left(1 - 18\Re_i\right)^{-\frac{1}{4}} \tag{54}$$

This expression can then be substituted into equation (52) to obtain equation (55).

$$\varphi_u = \left(1 - 18\Re_i\right)^{-\frac{1}{4}} \tag{55}$$

As $\Re_i$ is varied in convenient steps, pairs of values z/L', and φ_u are obtained from (54) and (55) that yield φ_u as a function of z/L' and that satisfy equation (48).

The last part of the definition of (39) is to integrate equation (50). To accomplish this, ζ is expressed as a function of φ_u and the integrand is transformed from a function of ζ to a function of φ_u.

From equation (50),

$$\zeta = \left((\varphi^*)^4 - 1\right)\left(\varphi^*\right)^{-3}/18 \tag{56}$$

- 21 -

and

$$\frac{d\zeta}{d\varphi^*} = \frac{4(\varphi^*)^3 (\varphi^*)^{-3}}{18} - \frac{3(\varphi^*)^{-4} ((\varphi^*)^4 - 1)}{18} \tag{57}$$

so that

$$\frac{1 - \varphi^*}{\zeta} \, d\zeta = \left(3 - \frac{3}{\varphi^*} - \frac{4 (\varphi^*)^3}{(\varphi^*+1)((\varphi^*)^2 + 1)} \right) d\varphi^* \tag{58}$$

In partial fraction form, the last term of equation (58) can be written as equation (59).

$$\frac{4(\varphi^*)^3}{(\varphi^* + 1)(\varphi^{*2} + 1)} = 4 - \frac{2}{1+\varphi^*} - \frac{2}{1+(\varphi^*)^2} - \frac{2\varphi^*}{1+(\varphi^*)^2} \tag{59}$$

The function, $\Psi(z/L')$, can then be represented by equation (60), and the integrations are straight forward as given by equation (61).

$$\Psi(z/L') = \int_1^{\varphi_u} \left(-1 - \frac{3}{\varphi^*} + \frac{2}{1+\varphi^*} + \frac{2}{1+\varphi^{*2}} + \frac{2\varphi^*}{1+\varphi^{*2}} \right) d\varphi^* \tag{60}$$

$$\Psi(z/L') = 1-\varphi_u - 3 \ln \varphi_u + 2 \ln \left((1+\varphi_u)/2 \right) + 2 \tan^{-1} \varphi_u - \frac{\pi}{2}$$

$$+ \ln \left((1+\varphi_u^2)/2 \right) \tag{61}$$

- 22 -

6.5 The Relationship Between z_o and u_*

The definition of the wind as a function of height below the height, h, is still not complete because the roughness length has still not been specified. The problem can be closed by giving a functional relationship between z_o and u_*. Cardone (1969) proposed the relationship given by equation (62a). Garratt (1977) has proposed equation (62b), and Pierson (1978) proposed the compromise between the two given by (62c). In these equations z_o is in centimeters and u_* is in cm/sec.

$$z_o = 0.684u_*^{-1} + 4.28 \times 10^{-5}u_*^2 - 0.0443 \qquad (62a)$$

$$z_o = 1.469 \times 10^{-5}u_*^2 \qquad (62b)$$

$$z_o = 0.3905u_*^{-1} + 1.6046 \times 10^{-5}u_*^2 - 0.01747 \qquad (62c)$$

(Note the typographical and drafting errors in 5A and Fig. 1 of Pierson (1978) which are corrected by 62a.)*

In TWINDX, z_o is in feet and u_* is in ft/sec for the actual calculations (a throwback to the original program from Thomasell and Welsh (1963)). For these units, these equations become (63a), (63b) and (63c).

$$z_o = '.3627 \times 10^{-4}u_*^{-1} + 1.3045 \times 10^{-3}u_*^2 - 1.4534z10^{-3} \qquad (63a)$$

$$z_o = 4.474 \times 10^{-4}u_*^2 \qquad (63b)$$

$$z_o = 4.203 \times 10^{-4}u_*^{-1} + 4.891 \times 10^{-4}u_*^2 - 5.73 \times 10^{-4} \qquad (63c)$$

---

*Most recent copies have been corrected.

- 23 -

The choice of any one of these relationships closes the problem, and makes it possible to evaluate the wind speed as a function of height given the average wind at any elevation and the air sea temperature difference.

There are some fundamental differences of philosophy involved in relating the SASS backscatter values to the friction velocity and the wind as measured at some fixed elevation abouve the sea surface. These differences have been discussed in Part 1 of this final report and in Appendix E. Since u_* is a difficult quantity to measure routinely, even if the model function is determined in terms of u_*, it will be necessary to use some relationship such as equation (62a), (62b) or (62c) to compute the wind that will be measured at the surface truth site for verification purposes.

It is also necessary to correct the wind at the chosen anemometer height to the effective neutral stability wind if the atmosphere is not neutrally stratified. For the same u_*, the actual wind will be stronger at the height z for a stable atmosphere and weaker for an unstable atmosphere. Conversely, for the same wind speed at the height z, the value of u_*' is higher in an unstable atmosphere and lower in a stable atmosphere, compared to the neutrally stratified atmosphere.

6.6 The Internal Boundary Condition

The Cardone model for the winds over the ocean surface is a two layer model. The wind above the level, h, is defined by a form of the Ekman spiral, as determined by the gradient wind, and the thermal wind. Below the level h the wind is defined by equation (36) and the accompanying definitions of L' and z_o.

24

The Cardone model matches the wind speed and direction for the upper level to the wind speed and direction for the lower level by setting them equal at the height, h, and by imposing the continuity of the wind shear at h. Let $\vec{V}_T(z)$ be the total wind above h, and $\vec{u}(z)$ be the Monin-Obukhoff wind below h. At the height, h, the internal boundary conditions are given by equations (64), (65), and (66).

$$\vec{V}_T(h) = \vec{u}(h) \tag{64}$$

$$\left. \frac{\partial \vec{V}_T(z)}{\partial z} \right|_{z = h} = \left. \frac{\partial \vec{u}(z)}{\partial z} \right|_{z = h} \tag{65}$$

$$K_u = K_M \text{ at } z = h \tag{66}$$

The procedure for satisfying these internal boundary conditions is illustrated by Figure 1A. Figure 1A is for the simpler case for which there is no variation of the gradient wind with height. It corresponds to barotropic conditions locally in the field.

The wind in the surface layer can be described by equation (36) and an unknown direction as in either equation (67) or (68).

$$u = \bar{u}(z) \cos \alpha \tag{67a}$$

$$v = \bar{u}(z) \sin \alpha \tag{67b}$$

$$\vec{u}(z) = \bar{u}(z) e^{i\alpha} \tag{68}$$

for $\quad 0 < z \leq h$

- 25 -

The barotropic condition can be treated simply. Since there is usually some contribution from the thermal wind, only a few of the points in an actual wind field will be solutions for this condition. In component form, the appropriate Ekman solution at and above the height, h, is given by equation (69) where the u component is parallel to the gradient wind. In complex notation, the same solution is given by equation (60) where G is the gradient wind.

$$u_{EKMAN} = G + e^{-a(z-h)} (\bar{u}(h) \cos(\alpha+ah-az) - G \cos(ah-az)) \tag{69a}$$

$$v_{EKMAN} = e^{-a(z-h)} (\bar{u}(h) \sin(\alpha+ah-az) - G \sin(ah-az)) \tag{69b}$$

$$\vec{V}_{EKMAN} = G + \bar{u}(h) \, e^{ah + i(\alpha + ah)} \left(e^{-a(1 + i)z} \right) - G \, e^{ah + iah} \left(e^{-a(1 + i)z} \right)$$

for $h \leq z < \infty$ $\qquad\qquad$ (70)

For (69), when $z = h$, the equations become

$$u_{EKMAN} = \bar{u}(h) \cos \alpha \tag{71a}$$

$$v_{EKMAN} = \bar{u}(h) \sin \alpha \tag{71b}$$

- 26 -

and (70) becomes

$$V_{EKMAN} = \bar{u}(h)\, e^{i\alpha} \tag{72}$$

If the wind from the surface to the height, h, is evaluated at
h, it should also have the magnitude, $\bar{u}(h)$, and the direction, α, to
impose the condition for the continuity of the vector wind with height.
The value of α for this condition is clearly unknown since the con-
dition can be satisfied for any angle.

The shear for the wind in the lower layer from equation (68) is
given by equation (73) at h.

$$\frac{\partial \vec{u}(z)}{\partial z} \bigg/_{z\,=\,h} = \frac{u_* \, h}{\kappa \, \varphi_u} \, e^{i\,\alpha} \tag{73}$$

The shear for the wind in the upper layer is given by equation (74)
at h.

$$\frac{\partial \vec{V}_{EKMAN}}{\partial z} \bigg/_{z\,=\,h} = \frac{\sqrt{2}\ a(1 + i)}{\sqrt{2}} \left(G - e^{i\alpha}\, \bar{u}(h) \right) \tag{74}$$

The right hand sides of equations (73) and (74) must be equal in
both direction and magnitude to satisfy equation (65).

The situation is illustrated in Figure 1A. The solid lines re-
present the vector winds. The dashed lines represent properties of
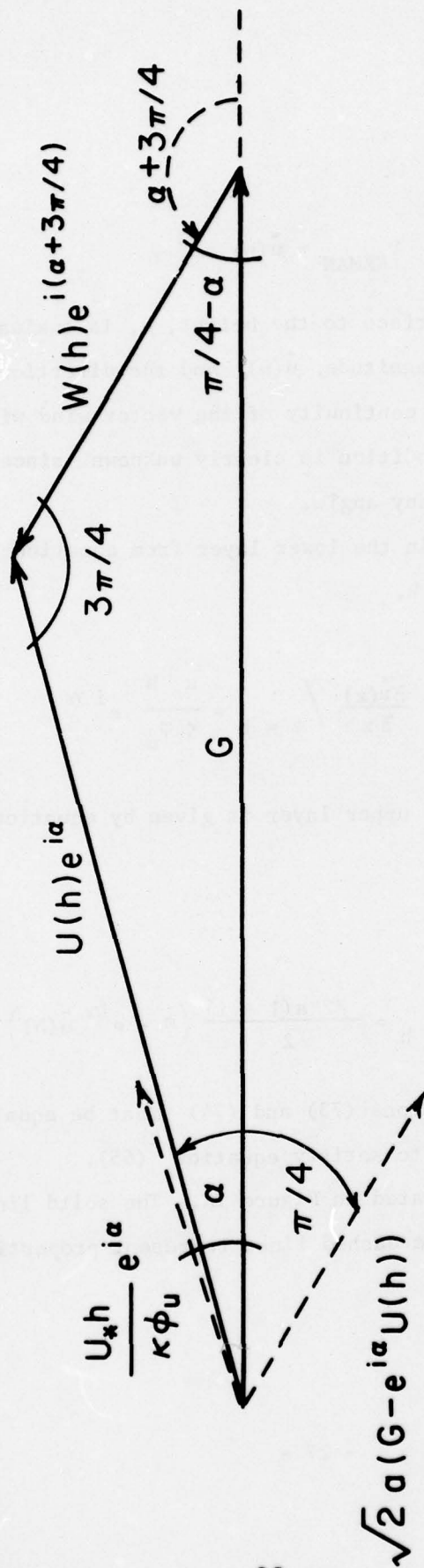
Figure 1a. The internal boundary conditions for the barotropic case for continuity in the vector wind and the vector wind shear.

the vector shears. The shear of the wind in the lower layer lies in the same direction as the vector wind. It is shown by an appropriate dashed line.

Although with different dimensions, the other dashed line must have the same direction as the difference vector given by (75).

$$\vec{W} = G - \vec{u}(h)\, e^{i\alpha} \tag{75}$$

But from equation (72), this difference vector is multiplied by $(1 + i)/\sqrt{2}$ which is the equivalent of rotating it $\pi/4$ radian (or $45°$) in the clockwise direction.[*] The vector shears can only be identical at the height, h, if the three interior angles of the triangle $\vec{G}$, $\vec{W}$, $\vec{U}$ are as shown in Figure 1A. One of the interior angles must equal $3\pi/4$ and since the difference in direction between the surface wind and the gradient wind is α, the remaining angle must be $\pi/4 - \alpha$.

These angular relationships then transform the problem of finding the properties of the wind in the surface layer to a problem in trigonometry that uses only the magnitude of the various vectors, $|\vec{G}|$, $|\vec{u}(h)|$ and $|\vec{W}(h)|$ and these angles.

The condition given by equation (66) can be satisfied by noting that

$$\kappa_M = \kappa\, u_* \, h \, (\varphi_u(h/L'))^{-1} = \kappa\, u_* \, B_o G/f\varphi_u(h/L') \tag{76}$$

at h which in turn yields the value of a as in equation (77)

$$a = f\left[\varphi_u(h/L')/2\kappa\, u_* \, B_o G\right]^{\frac{1}{2}} \tag{77}$$

---

[*] It is slightly displaced for clarity in the figure.

- 29 -

The magnitude of $G - e^{i\alpha} \bar{u}(h)$ is defined to be $|\vec{W}(h)|$ and from (73), (74) and (16), it follows that

$$|\vec{W}(h)| = u_* \, f \, \varphi_u(z/L')//2 \, \kappa \, B_o G_a$$

$$= u_*^{\frac{1}{2}} \left[\varphi_u(h/L') / \kappa \, B_o G \right]^{\frac{1}{2}} \tag{78}$$

The law of sines applied to $|\vec{U}(h)|$ and $|\vec{G}|$ in Figure 1A yields

$$\frac{|\vec{u}(h)|}{|\vec{G}|} = \sqrt{2} \sin\left(\frac{\pi}{4} - \alpha \right) \tag{79}$$

When applied to $|\vec{W}(h)|$ and $|\vec{G}|$, it yields

$$\frac{|\vec{W}(h)|}{|\vec{G}|} = \sqrt{2} \sin \alpha \tag{80}$$

When equation (78) is substituted into equation (80), the result is equation (81)

$$\left(\frac{u_*}{G} \right)^{\frac{3}{2}} = \left(\frac{2 \, \kappa \, B_o}{\varphi_u(h/L')} \right)^{\frac{1}{2}} \sin \alpha \tag{81}$$

or, equivalently, equation (82).

$$\frac{u_*}{G} = \left[2 \, \kappa \, B_o (\sin \alpha)^2 / \varphi_u(h/L') \right]^{\frac{1}{3}} \tag{82}$$

With equation (36) evaluated at $z = h = B_o G/f$, equation (77) becomes equation

$$\frac{u_*}{G} = \sqrt{2}\; \kappa\; \sin\left(\frac{\pi}{4} - \alpha\right) \Bigg/ \left(\ell n\left(\frac{B_o G}{f z_o}\right) - \Psi(h/L')\right) \qquad (83)$$

Equations (82) and (83), along with $\underline{a}$ relationship for z_o as a function of u_* (in the program 63a or b or c) and the equation for L' as in equation (37) form a set of four equations in four unknowns (or with z_o eliminated by expressing it as a function of u_*) a set of three equations in three unknowns. They are written out completely in equations (84), (85), and (86)

$$\frac{u_*}{G} = \left[2\kappa\, B_o (\sin \alpha)^2 \Big/ \varphi_u (B_o G/f L')\right]^{\frac{1}{3}} \qquad (84)$$

$$\frac{u_*}{G} = \sqrt{2}\; \kappa\; \sin\left(\frac{\pi}{4} - \alpha\right) \Bigg/ \left(\ell n\left(\frac{B_o G}{f z_o(u_*)}\right) - \Psi(B_o G/f L')\right) \qquad (85)$$

$$L' = \frac{u_*^2\; \bar{\theta}\left(\ell n\left(z_a/z_o(u_*)\right) - \Psi(z_a/L')\right)}{\kappa^2\, g(\theta_a - \theta_s)} \qquad (86)$$

For this particular model φ_u is found from (47) for a stable atmosphere and from (54) and (55) for an unstable atmosphere, and $\Psi(h/L')$ (or z_a/L') is found from $\varphi_u(h/L')$. The unknowns in (84), (85) and (86) are u_*, α, and L'. The values of G, f, $\bar{\theta}$, θ_a and θ_s are obtained from the input fields, and, of course, the various constants are known. The value of z_a is 10 meters. Once the values of u_*, α and L' are found, the wind at any height from the surface to the gradient wind level can be computed.

The internal boundary condition for the baroclinic case is illustrated in Figure 1B. The vector wind from the surface to h is given by equation (68), and the shear at h computed in the surface layer is given by (73).

The vector wind above h is given by equation (87)

$$\vec{V}_{TOTAL} = G + (z-h)\left|\frac{dG}{dz}\right|e^{i\eta} + \bar{u}(h)\ e^{ah+i(\alpha+ah)}\left(e^{-a(1+i)z}\right)$$

$$- G\ e^{ah+iah}\left(e^{-a(1+i)z}\right) \tag{87}$$

The shear of the wind at h calculated from the total wind above h is given by (88).

$$\frac{\partial\vec{V}_{TOTAL}}{dz}\ \Big/_{z=h} = \left|\frac{dG}{dz}\right|e^{i\eta} + a(1+i)\left(G-\bar{u}(h)e^{i\alpha}\right)$$

$$= \left|\frac{dG}{dz}\right|e^{i\eta} + \sqrt{2}\ a\left(G-\bar{u}(h)e^{i\alpha}\right)e^{i\ \pi/4} \tag{88}$$

In Figure 1B, an attempt is made to clarify one of the more incomprehensible figures in the Cardone model by keeping the vector wind shear balance separate from the vector wind balance. Dashed vectors represent shears, and solid vectors represent winds. The sum of $\vec{W}(h)$ and $\vec{G}$ must equal $\vec{u}(h)$, as shown, to satisfy the internal boundary condition given be equation (64).

As shown by the dashed line, the shear of the wind in the surface layer lies parallel to the surface wind. Since the shear has a different dimension, the fact that it is drawn to the same length is at the moment
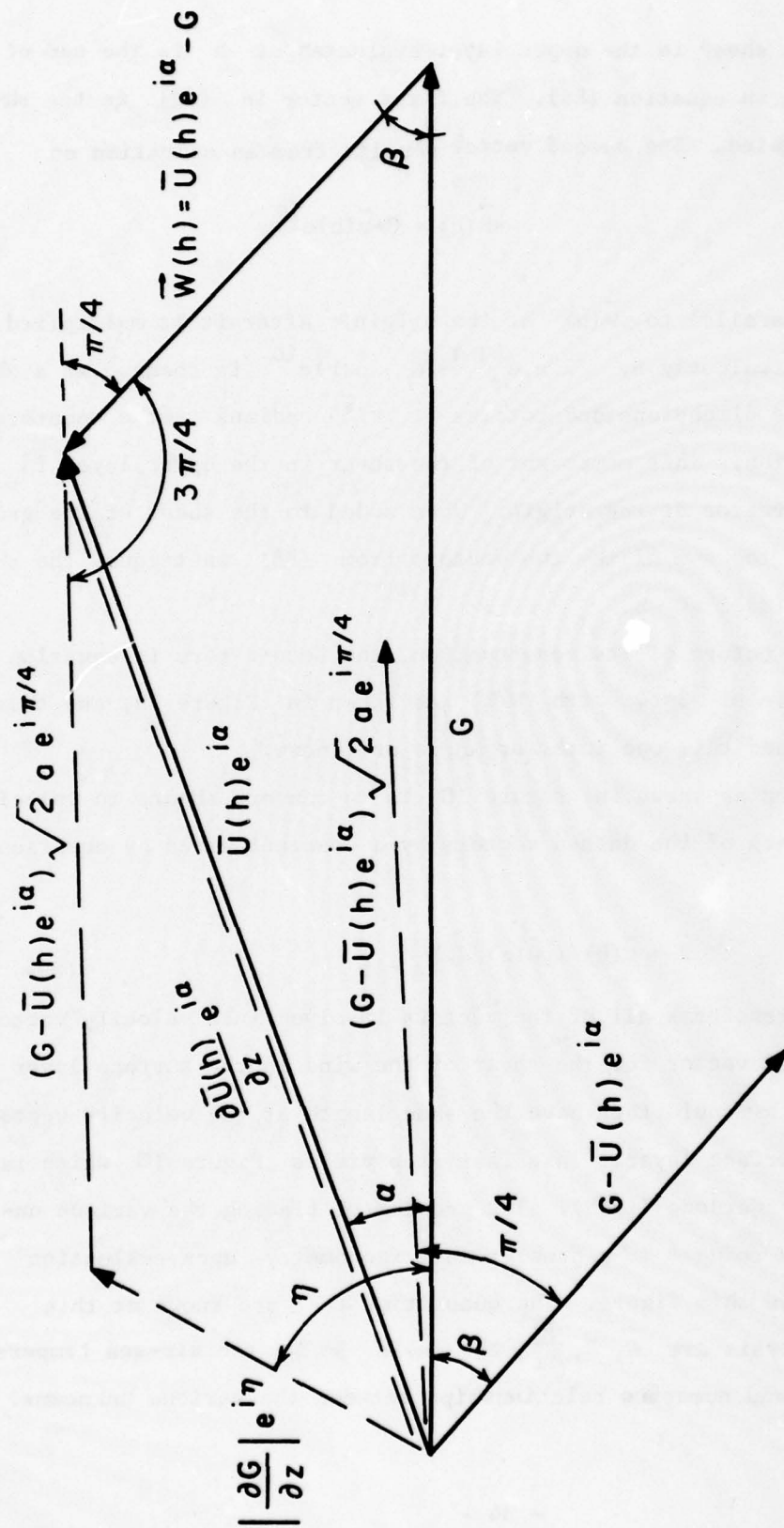
Figure 1b. The internal boundary conditions for the baroclinic case for continuity in the vector wind and the vector wind shear.

irrelevent. The shear in the upper layer evaluated at h is the sum of two
vectors as shown in equation (88). The first vector in (88) is the shear
of the gradient wind. The second vector results from an operation on

$$-\vec{W}(h) = G-\bar{u}(h)e^{i\alpha}$$

which is shown parallel to $\vec{W}(h)$ at the origin. After it is multiplied by
$a(1 + i)$, or equivalently by $\sqrt{2}\ a\ e^{i\pi/4}$, $G - \bar{u}(h)e^{i\alpha}$ is changed to a shear,
which changes its dimensions and rotates it $\pi/4$ radians in the counter-
clockwise direction. This component of the shear in the upper layer is
also shown as a vector at the origin. When added to the shear of the gradient
wind (as shown) the sum of the two vectors from (88) must equal the shear
for the surface layer at h.

By the very nature of its construction, the second term in equation (88)
must make an angle of $3\pi/4$ with $\vec{W}(h)$ as shown in Figure 1B, and thus
the value of η and this one interior angle are known.

The next step as shown in Figure 1C is to convert shears to velocities
by multiplying each of the dashed vectors by a constant given by equation (89).

$$P = \bar{u}(h)/(\partial\bar{u}(z)/dz)\Big/_{z} = h \tag{89}$$

This step transforms all of the vectors involved into velocity vectors
so that the dashed vector for the shear of the wind in the surface layer
as evaluated at h would then have the same length at the velocity vector
at h for the surface layer. This last step yields Figure 1C which is
the one given by Cardone (1969). The problem of finding the various un-
known quantity is reduced to a problem in trigonometry upon evaluation
of the unknowns in this figure. The quantities that are known at this
stage of the analysis are $\vec{G}$, η, $\dfrac{d\vec{G}}{dz}$, the angle $3\pi/4$, the air-sea tempera-
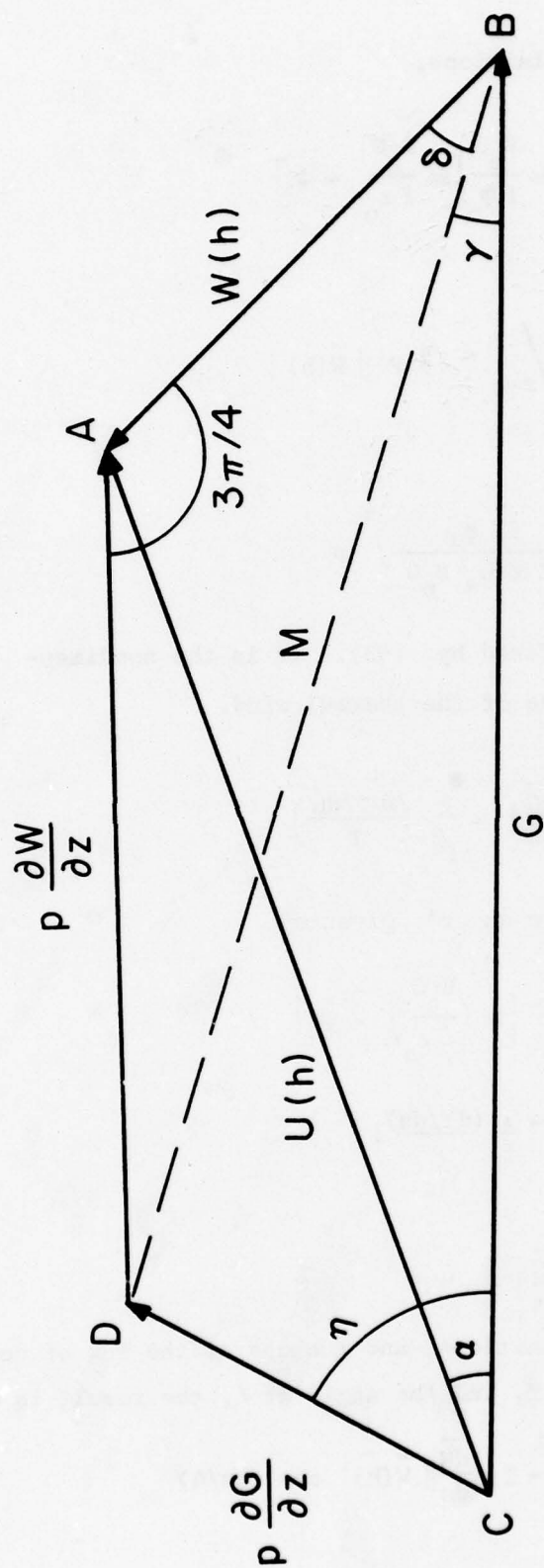ture difference and numerous relationships between the various unknowns.

- 34 -

Figure 1c. The vector diagram for the internal boundary condition upon converting shears to velocities by means of the quantity, P.

From the available definitions,

$$p = \frac{B_o G}{f \varphi_u}\left[\ell n \; \frac{B_o G}{f z_o} \; - \Psi\right] \tag{90}$$

and from

$$p \left| \frac{d\vec{W}}{dz} \right| \bigg/_{z=h} = \sqrt{2} \; p' \left| \vec{W}(h) \right| \tag{91}$$

so that

$$p' = \left(\frac{f^2 \, \varphi_u}{2 \, \kappa \, u_* \, B_o G} \right)^{\frac{1}{2}} p \tag{92}$$

The quantity, r, is defined by (93). It is the nondimensional form for the magnitude of the thermal wind.

$$r = \frac{1}{f} \left| \frac{d\vec{G}}{dz} \right| \; = \frac{g}{f^2} \left(\frac{d \; T/dn}{T} \right) \tag{93}$$

Also it is possible to define an r' given by

$$r' = \frac{r \, B_o}{\varphi_u} \left[\ell n \left(\frac{B_o G}{f z_o} \right) \; - \Psi \right]$$

$$= p f \left| \frac{1}{f} \; \frac{(dT/dn)}{T} \right| \tag{94}$$

so that

$$p \left| \frac{d\vec{G}}{dz} \right| = r' \, G \tag{95}$$

From these various definitions, and the use of the law of cosine for the triangle with the side, M, and the angle at A, the result is equation (96),

$$M^2 = \left| p \; \frac{d\vec{W}}{dz} \right|^2 + \left| \vec{W}(h) \right|^2 - 2 \, p \left| \frac{d\vec{W}}{dz} \right| \left| \vec{W}(h) \right| \cos (3\pi/4) \tag{96}$$

- 36 -

which can be reduced to

$$M^2 = |\vec{W}(h)|^2 \left(2(p')^2 + 2p' + 1\right) \tag{97}$$

$$= |\vec{W}(h)|^2 s^2$$

For the triangle with the side M and the angle, η,

$$M^2 = \left| p \frac{d\vec{G}}{dz} \right|^2 + |\vec{G}|^2 - 2 p \left| \frac{d\vec{G}}{dz} \right| |\vec{G}| \cos \eta \tag{98}$$

which can be reduced to

$$M^2 = |\vec{W}(h)|^2 \left(1 + (r')^2 - 2r' \cos \eta\right) = |\vec{W}(h)|^2 q^2 \tag{99}$$

From triangle, ABD, the law of sines, and equation (97),

$$\sin \delta = \frac{p|d\vec{W}/dz|}{\sqrt{2} M} = p'/s \tag{100}$$

From triangle, BCD the law of sines, and equation (99),

$$\sin \gamma = \frac{p|d\vec{G}/dz|}{M} \sin \eta = \frac{r'}{q} \sin \eta \tag{101}$$

From triangle ABC, and the law of sines,

$$|\vec{u}(h)| = |\vec{W}(h)| \sin (\delta + \gamma)/\sin \alpha \tag{102}$$

and from the same triangle and law of cosines,

$$|\vec{u}(h)|^2 = |\vec{G}|^2 + |\vec{W}(h)|^2 - 2|\vec{G}| |\vec{W}(h)| \cos (\delta + \gamma) \tag{103}$$

- 37 -

Also from the triangle involving α,

$$|\vec{W}(h)|^2 = |\vec{u}(h)|^2 + |\vec{G}|^2 - 2|\vec{u}(h)||\vec{G}|\cos\alpha \qquad (104)$$

From (102) and (104),

$$\tan\alpha = \frac{2|\vec{G}||\vec{W}(h)|\sin(\gamma+\delta)}{|\vec{G}|^2 + (\vec{u}(h)|^2 - |\vec{W}(h)|^2} \qquad (105)$$

Equation (105) can be transformed to equation (106) by means of equations (103) and (99).

$$\tan\alpha = \frac{\sin(\delta+\gamma)}{\dfrac{s}{q} - \cos(\delta+\gamma)} \qquad (106)$$

From the definition of $\bar{u}(h)$, from (102) and from

$|\vec{W}(h)| = q|\vec{G}|/s$, the result is equation (107).

$$\frac{u_*}{|\vec{G}|} = \frac{\kappa\, q\, \sin(\delta+\gamma)}{s\,\sin\alpha\left[\ell n\left(\dfrac{B_o\, G}{f z_o}\right) - \Psi(h/L'\right]} \qquad (107)$$

Matching the velocity and shear at the height, h, given by equation (16) can lead to problems for light gradient winds because h can be less than 19.5 meters, which is the height at which the wind is to be specified. There are two possible ways to treat the problem when h is less than 19.5 meters and, yet, when the short cut solution for very light winds is not applied. One would be to use the computed value of h and obtain the wind at 19.5 meters from equation (87) since z = 19.5m

would be greater than h. The other way would be to set h equal to 19.5m and to be sure to use that height in all subsequent calculations. To demonstrate which of the two would be best would require very careful measurements of the variation of the time averaged wind with height for the first 30 meters above the sea surface.

For TWINDX, the choice was to set h = 19.5m if it was calculated to be less than this value and to use h = 19.5 meters in all subsequent equations for the calculation of the unknown quantities.

The various equations therefore have to be put into a form where h appears for B_oG/f whenever the height is needed.

They have been presented above in the order of their derivation, and so as to demonstrate the procedure for solution, some of them are repeated here in a different order.

$$h = B_oG/f, \text{ or } 19.5\text{m (whichever is greater)} \tag{108}$$

$$z_o = z_o(u_*) \tag{109}$$

$$L' = \frac{u_*^2 \, \bar{\theta} \, (\ell n \, (z_a/z_o) - \Psi \, (z_a/L'))}{\kappa^2 g \, (\theta_a - \theta_s)} \tag{110}$$

$$\frac{z}{L'} = R_i \, (1 - 18 \, R_i)^{\frac{1}{4}} \tag{111}$$

$$\varphi_u = (1 - 18 \, R_i)^{-\frac{1}{4}} \tag{112}$$

$$\Psi (z/L') = 1 - \varphi_u - 3 \ell n \; \varphi_u + 2 \ell n \; ((1 + \varphi_u)/2) + 2 \; \tan^{-1} \varphi_u - \pi/2$$
$$+ \ell n \; ((1 + \varphi_u^2)/2) \tag{113}$$

$$p = \frac{h}{\varphi_u} (h/L') \; \ell n \; (h/z_o) - \Psi \; (h/L')) \tag{114}$$

$$p' = \left(\varphi_u f/2\kappa \; u_* \; h \right)^{\frac{1}{2}} p \tag{115}$$

$$r' = p \; f \; \frac{1}{f} \; \frac{d \, T}{d \, n} \; \frac{1}{T} \; /G \tag{116}$$

$$s = \left(2 \; (p')^2 + 2 \, p' + 1 \right)^{\frac{1}{2}} \tag{117}$$

$$q = \left(1 + (r')^2 - 2 \; r' \; \cos \eta \right)^{\frac{1}{2}} \tag{118}$$

$$\delta = \sin^{-1} \; (p'/s) \tag{119}$$

$$\gamma = \sin^{-1} \; (r' \; \sin \eta /q) \tag{120}$$

$$\alpha = \tan^{-1} \left(\frac{\sin \; (\delta + \gamma)}{\frac{s}{q} - \cos \; (\delta + \gamma)} \right) \tag{121}$$

$$u_* = G \; \frac{\kappa \; q \; \sin \; (\delta + \gamma)}{s \; \sin \alpha \; (\ell n \; (h/z_o) - \Psi \; (h/L'))} \tag{122}$$

Equations (108) through (122) are the system of equations that
need to be solved in order to find u_*, L', and α. These quantities

then define the wind speed and direction from the surface to h. Also since $K_M = \kappa u_* h(\varphi_u)^{-1}$, the vector wind in equation (87) above h to the gradient wind level is known.

The procedure is to compute the geostrophic wind speed and direction and modify it on the basis of isobaric curvature to the gradient wind speed. Next the thermal wind is nondimensional form as in (93) is found along with the angle, η, measured counterclockwise from the surface gradient wind direction. The result of (93) is used to find the required term for (94), or (116). The other terms of that equation are defined by equation (114).

In the present version, $\theta_a - \theta_s$ is kept less than or equal to 4° Celsius. This can be relaxed by changing one line of code if the behavior of the model for very stable air is desired.

Known at the start of the calculation are h, G, f, $\dfrac{d\vec{G}}{dz}$, θ_a and θ_s.* Then u_*, L', and α, and from these $\bar{u}$ (19.5), for both a neutrally stratified atmosphere and for the Monin-Obukhoff profiles can be computed.

If $\lvert G \rvert$ is less than 2.51 m/s (8.25 ft/sec), the calculation is bypassed, the wind at 19.5m is set equal to 0.7G and the direction is 15° toward low pressure. u_* is set to 0.0220G. L' is set to zero (a convention for an infinite value). The next grid point is then processed.

If the wind speed is greater than 2.51 m/s, a first guess for u_* of 0.0245G is made, the thermal wind is assumed zero and is set to zero.

If $\lvert \theta_a - \theta_s \rvert$ is greater than 1^oC the values for L', Ψ (z/L') and φ_u(z/L') are found in later calculations, if not the neutral stability profile is used.

For neutral stability, L' is flagged as zero, Ψ is zero, and φ_u is one. The values of p (114), p' (115), s (117), r' (which is zero (116))

---

* $\dfrac{d\vec{G}}{dz}$ yields $\left| \dfrac{d\vec{G}}{dz} \right|$ and η.

$q = 1$, δ (117), $\gamma = 0$, α (121) and u_* (122) are found. These equations reduce to the barotropic case under the assumed conditions. The result is a value of α and new value of u_*, which differs from 0.0245G.

For the next cycle, the new value of u_* is used and thermal wind effects are included. The values of Ψ, φ_u, and L' are known. After several loops through the equations, if the last two calculations of u_* differ by less than 0.05 ft/sec, the last value of u_* is used along with α and the most recently obtained value of L'. The wind speed and direction at 19.5 meters are found, converted to m/s and written in an output field.

For non-neutral conditions, the first guess for u_* is the same as before. A first guess for L' is found from (110) with Ψ equal to zero. Then with this guess h/L' is used to find $\Psi(h/L')$ and $\varphi_u(h/L')$ in a subroutine from (111), (112) and (113). These values are then used to step through (114) through (122) and to obtain a new value of u_* (with thermal wind effects omitted). The old value of L' and the new value of u_* are then used to get a new value of L', calculated at an anemometer height of 10 meters, and new values of Ψ and φ_u. The thermal wind effects are included on the next pass and a new value of u_* is obtained. After a number of cycles through the equations, two successive values of u_* will differ by less than 0.05 ft/sec. The final values of u_*, α and L' are then used to define the wind at 19.5 meters from equation (36) for both the non-neutral case and the neutral case.

6.7 The Gradient Wind Level

The height at which the wind vector first parallels the contours of a constant pressure surface can be found by solving for the height, z, in equation (69b) that causes v to vanish. The wind will equal the Ekman component parallel to the surface isobars plus the value of (z-h) (d $\vec{G}$/dz) at that height. The term in parenthesis in (69b) can be re-written as

$$A \sin (\tan^{-1} B - (a h - a z)) \quad \text{where}$$

$$A = \left(\left(\bar{u}(h) \right)^2 - 2 G \ \bar{u}(h) \cos \alpha + G^2 \right)^{\frac{1}{2}} \tag{123}$$

and

$$\tan^{-1} B = \tan^{-1} \left(\frac{\bar{u}(h) \sin \alpha}{G - \bar{u}(h) \cos \alpha} \right) \tag{124}$$

The term vanishes when

$$\tan^{-1} B - a h + a h_G = \pi \tag{125}$$

where h_G is the height of the gradient wind level.

Thus

$$h_G = h + \frac{\pi}{a} - \frac{1}{a} \tan^{-1} \left(\frac{\bar{u}(h) \sin \alpha}{G - \bar{u}(h) \cos \alpha} \right) \tag{126}$$

For the classical Ekman spiral, this height is π/a. The other two terms tend to cancel somewhat.

- 43 -

For the special case of a neutrally stratified barotropic atmosphere, the term on the right equals $\frac{\pi}{4} - \alpha$ and so equation (126) becomes (127).

$$h_G = \left(\frac{3\pi}{4} + \alpha\right) a^{-1} + h \qquad (127)$$

In turn, this can be expressed as

$$h_G = \left(\frac{3\pi}{4} + \alpha\right)\left(\frac{2\kappa}{f}\right)^{\frac{1}{2}}\left(u_* h\right)^{\frac{1}{2}} + h \qquad (128)$$

and from equation (84) and the definition of h

$$h_G = \left(1 + \left(\frac{3\pi}{4} + \alpha\right) \frac{(2\kappa)^{\frac{2}{3}}}{B_o^{\frac{1}{3}}} \left(\sin \alpha\right)^{\frac{1}{3}}\right) h \qquad (129)$$

or

$$h_G = \left(1 + \left(\frac{3\pi}{4} + \alpha\right)\left(13.08\right)\left(\sin \alpha\right)^{\frac{1}{3}}\right) h \qquad (130)$$

For $\alpha = 15^{\circ}$, (or $\pi/12$ radians), $h_G \cong 22.8h$, which seems to be reasonable.

6.8 Features of the Model

Some of the features of the model are illustrated by Figures 2, 3 4, 5, and 6. In Figure 2, the surface isobaric pattern of an extratropical cyclone is sketched along with heights of a constant pressure surface and three "surface" winds at A, B and C. As is typical of a low, the low aloft lies to the west northwest of the surface low, which would cause the winds above C to veer and those above A to back with height.
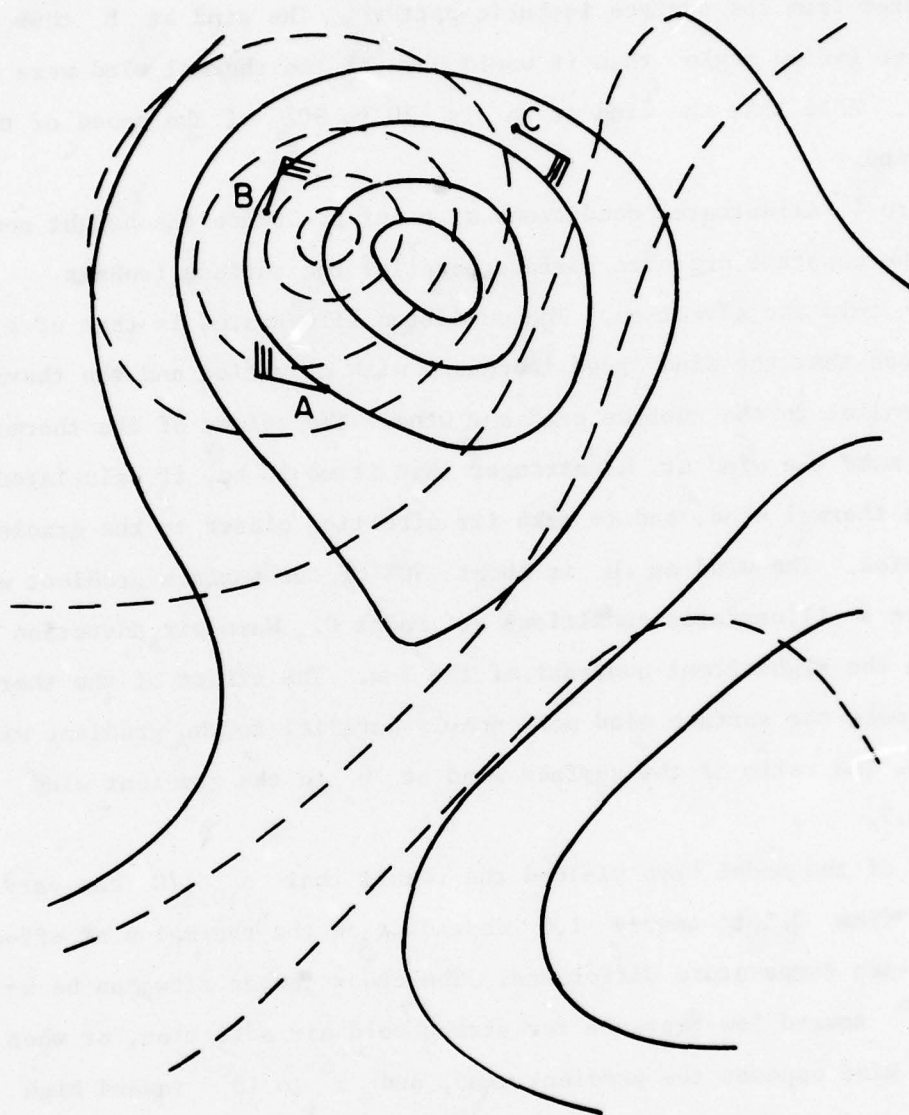
- 44 -

Figure 2. Sketch of surface winds, surface isobars, and a
constant pressure surface for an extratropical cyclone.

Figure 3 illustrates conditions at point A. There is cold air advection at A, and the thermal wind causes the wind at the gradient wind level to shift counterclockwise relative to the direction of the gradient wind computed from the surface isobaric pattern. The wind at h thus has a larger inflow angle than it would have if the thermal wind were not considered. Note that the wind at h is 70 to 80% of the speed of the gradient wind.

Figure 4 illustrates conditions at Point B. Since the height contours of the constant pressure surface parallel the surface isobars there is no cold air advection. The condition illustrated is that of a cold low such that the wind speed increases with elevation and the thermal wind is parallel to the surface gradient wind. The effect of the thermal wind is to make the wind at h stronger than it would be, if calculated without the thermal wind, and to make its direction closer to the gradient wind direction. The wind at h is about 90% of the surface gradient wind.

Figure 5 illustrates conditions at Point C. Warm air advection is shown in the right front quadrant of the low. The effect of the thermal wind is to make the surface wind more nearly parallel to the gradient wind and to leave the ratio of the surface wind at h to the gradient wind at about 0.7.

Tests of the model have yielded the result that $u_{19.5}/G$ can vary all the way from 0.5 to nearly 1.0 depending on the thermal wind effect and the air-sea temperature difference. The cross isobar flow can be as high as 30° toward low pressure for strong cold air advection, or when the thermal wind opposes the gradient wind, and 5° to 10° toward high pressure in regions of very strong warm air advection. A surface wind blowing toward high pressure would be treated as incorrect in most analysis schemes. A sample analysis on a 63 by 63 grid for January 9, 1974 is shown in Figure 6.
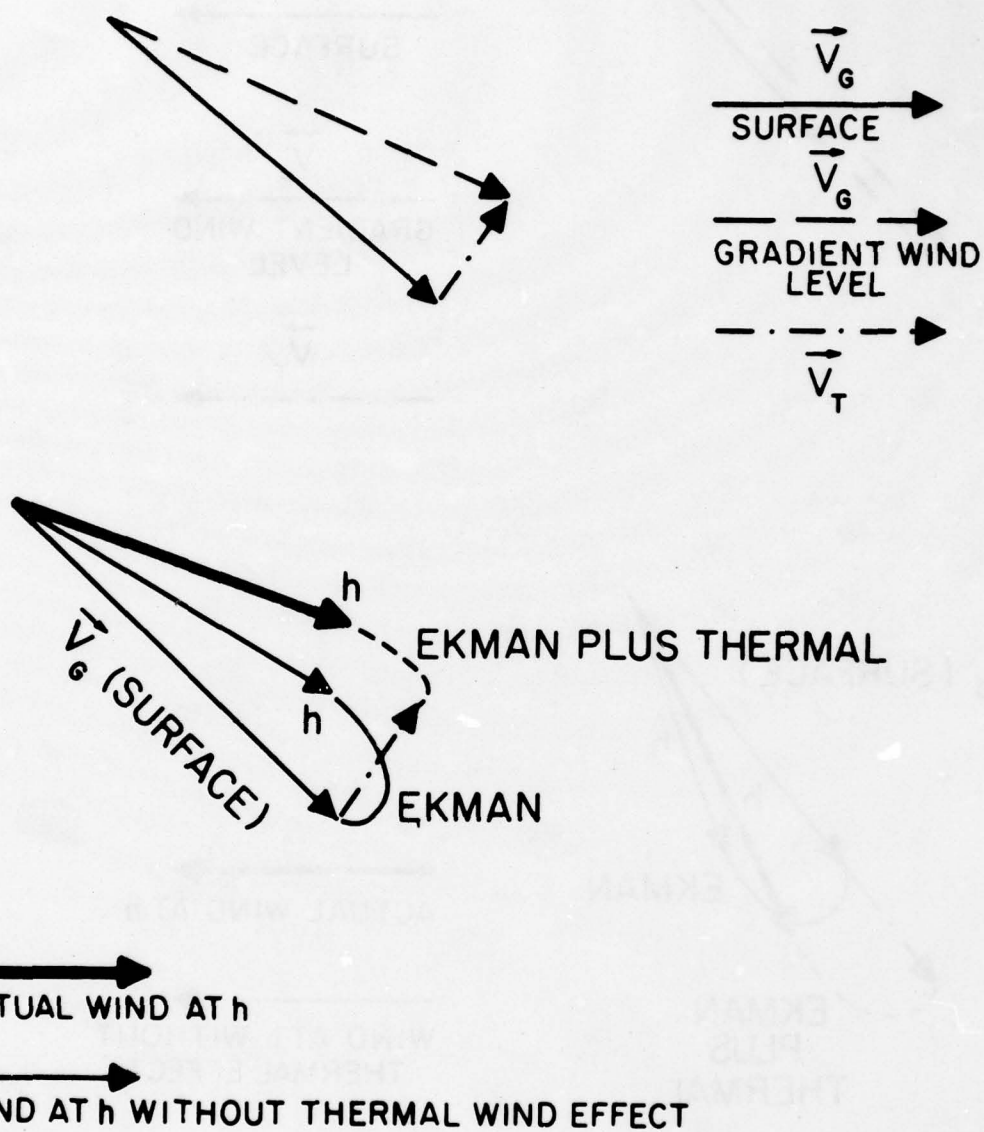
Figure 3. The effect of cold air advection in increasing cross-isobar flow for the surface wind.

$$\vec{V_G}$$
SURFACE

$$\vec{V_G}$$
GRADIENT WIND
LEVEL

$$\vec{V_T}$$

V_G (SURFACE)

h

h

EKMAN

EKMAN
PLUS
THERMAL

ACTUAL WIND AT h

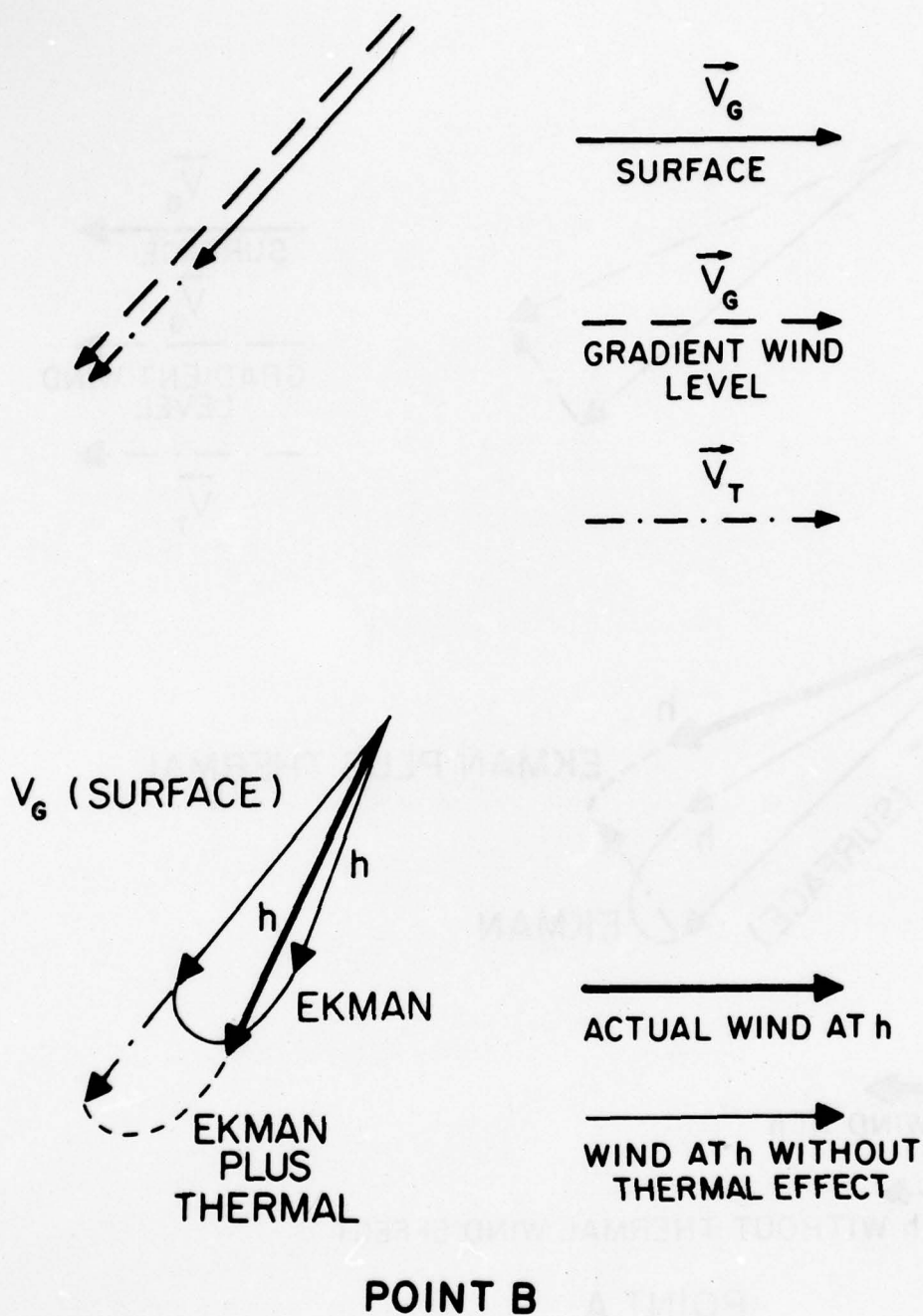WIND AT h WITHOUT
THERMAL EFFECT

POINT B

Figure 4. The effect of a cold low in increasing
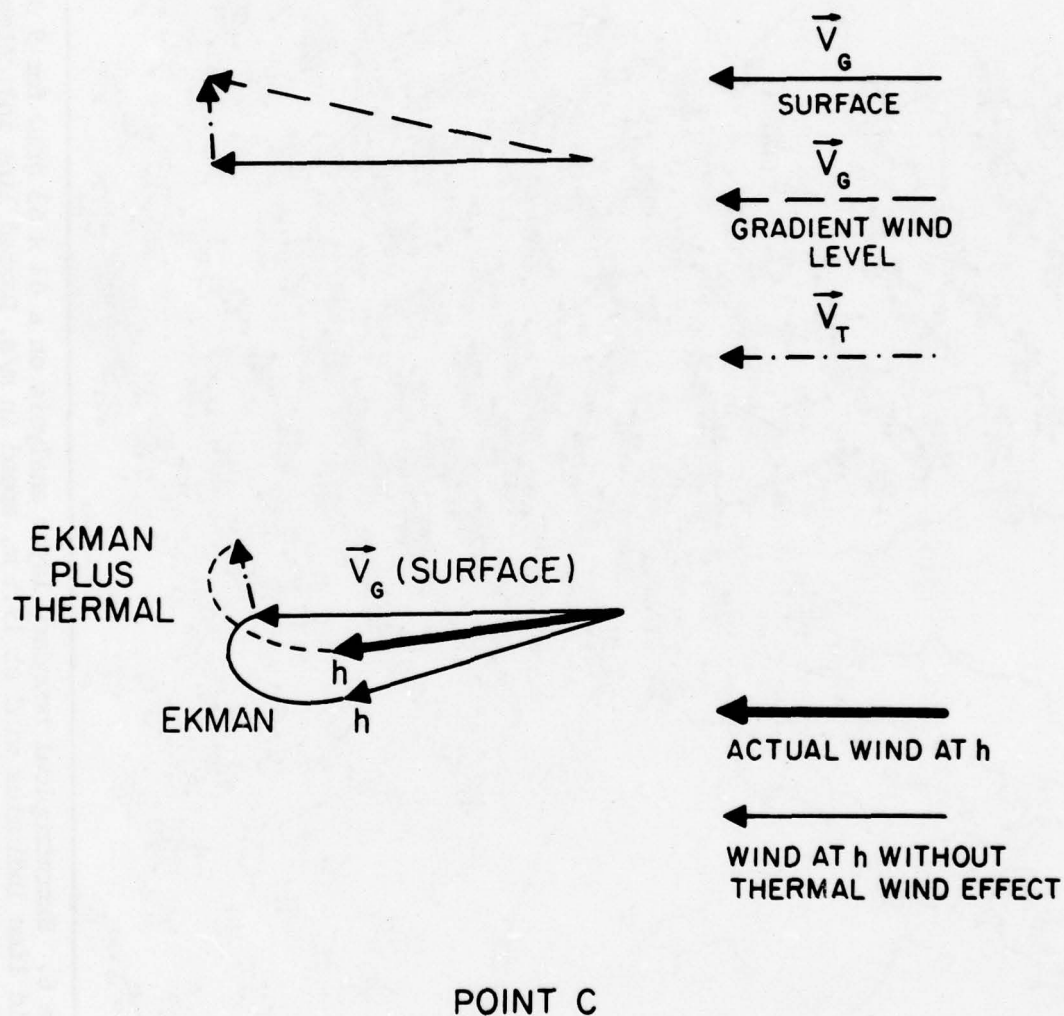the speed of the surface wind.

- 48 -

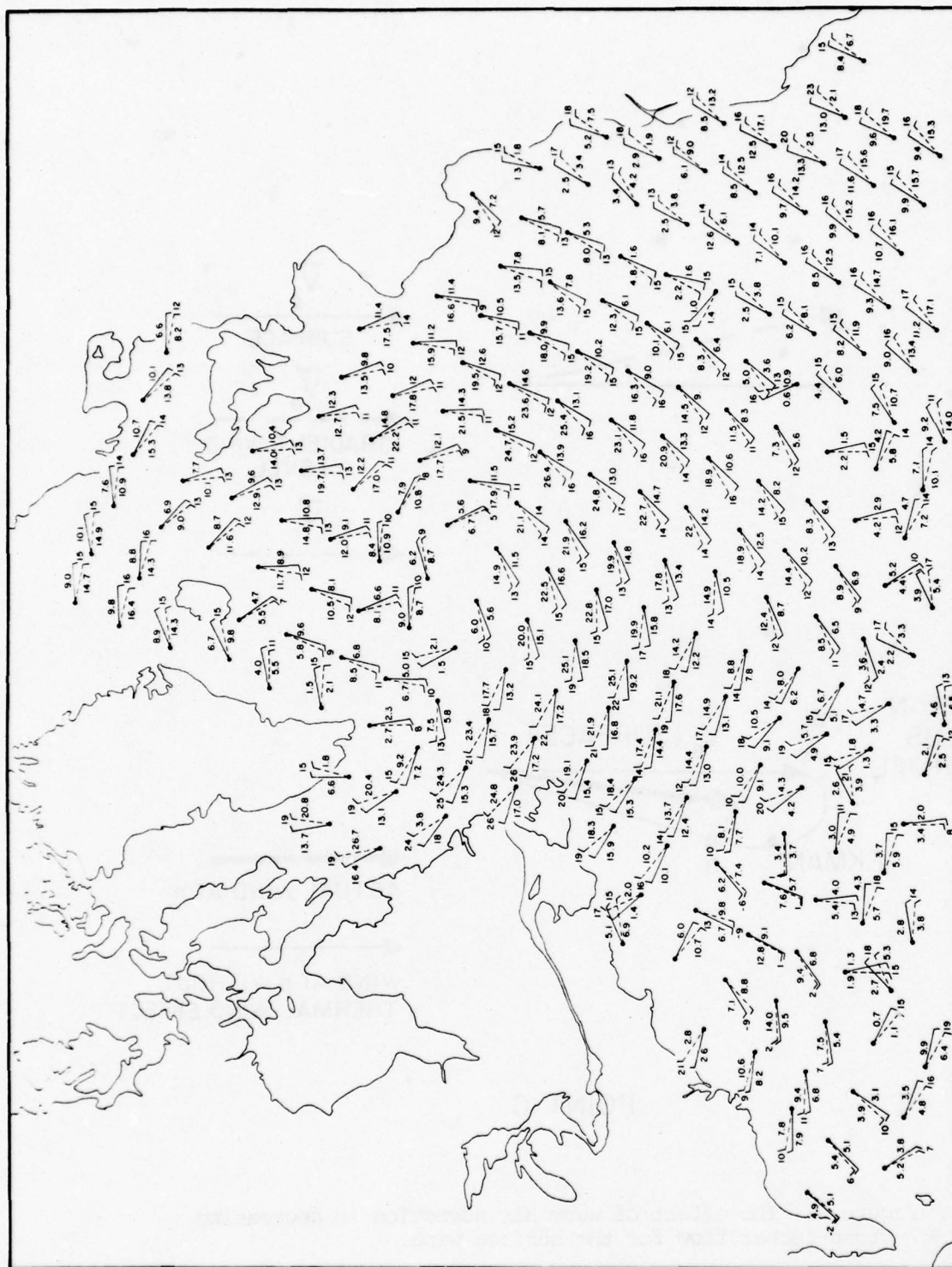Figure 5. The effect of warm air advection in decreasing cross-isobar flow for the surface wind.

Figure 6. Extratropical boundary layer analysis on a 63 x 63 grid for 9 Jan 1974, 18Z. Solid line indicates wind at 19.5 m, speed in m/s. Dashed line indicates gradient wind, speed in m/s. The integer is the angle between surface wind and gradient wind.

This range of 40°, or so, in the cross isobar direction and a variability in magnitude from 0.5G to 1.0G, centered on a value of about 0.7G compares favorably with the unexplained variances in the study by Thomasell and Welsh (1963). It remains to be seen how well the model will fit the more accurate winds to be found by SEASAT.

6.9 Variations and Potential Sources of Improvement

Variations of the present model can consist of increasing the upper bound on the magnitude of the nondimensional thermal wind now set at 100, and using other representations for $\Psi(z/L')$ and $\varphi_u(z/L')$. These combined with three different z_o versus u_* relationships provide a wide variety of outputs for the same input.

Allowing h to be less than 19.5 and calculating $\vec{u}(19.5)$ in the upper layer would be another modification. The vector wind stress would then differ in direction from the measured wind direction if the wind was measured at 19.5m, or higher (this should be checked in the SASS verification program).

Sensitivity tests for all of these permutations and combinations would be lengthy and expensive. Tests of the three different z_o versus u_* relationships did not produce dramatic changes in the output.

According to Brown (1978), "it is known that the velocity profile obtained from the Ekman-Taylor solution is unstable to infinitesimal perturbations in positive, neutral and even in a range of negative buoyancy stratifications....." However...." the flow is stable to finite perturbations, forming an equilibrium secondary flow." This secondary flow when added to the Ekman-Taylor solution modifies the shape of the Ekman spiral with less turning in unstable stratification

and greater turning through the PBL in stable stratifications. A modified Ekman spiral taking into account this secondary effect might be an improvement over the present model. Equations (70) and (87) would have to be modified, which in turn would modify all terms involving $\vec{W}(h)$. In Brown (1978), this secondary effect is treated as an additive constant.

One of the results of Brown (1978) for u_*/G determined over ice can be contrasted with these results for u_*/G over water for neutral stability. Brown given equation (131)

$$\frac{u_*}{G} = \frac{\kappa}{\ln E - 1.9} (\cos \alpha - 0.67 \sin \alpha) \qquad (131)$$

Compared to equation (84) for the barotropic case, one equation (equation (84)) predicts that u_*/G increases with increasing α, whereas the other, equation (131), predicts that u_*/G decreases with increasing α. Intuitively, one might expect that an increased surface stress would lead to an increased inflow angle, and so equation (131) seems strange.

For the baroclinic case, numerous factors determine the value of u_*/G other than just the inflow angle. It is not clear how the two relationships then compare except to note that the Brown model does not appear to treat the baroclinic case and that the example given above for the baroclinic case seem to yield reasonable results.

Brown (1978) also states that the "horizontal"? wavelengths of the eddies in the PBL are twice the height of the PBL, which could provide some useful information on the adequacy of the 10 to 20 minute time average anemometer winds that will be used to verify space averaged SASS winds. This scale of eddy sizes is clearly well averaged by a SASS cell.

7. THE WINDS IN THE TROPICS

7.1 Introduction

The location of the intertropical convergence zone and the doldrums and the description of variations from day to day of the trade winds are difficult problems when attempted for synoptic purposes as inputs to a numerical weather prediction model. Data density, prior to remote sensing techniques, left much to be desired. Moreover, the relationship between the field of mass and the winds, which for extratropical regions depends so strongly on coriolis effects, has not been well understood.

An intensification of scientific efforts in the study of the winds in the tropics, such as BOMEX and other studies, has focused on the importance of cloud physics in describing the circulations of the tropics. A note provided to the SASS team by V. Wong and T. N. Krishnamurti via P. M. Woiceshyn, provides a start for an operational way to describe the winds in the tropics over the ocean on the basis of additional field variables, one of which is the height of the lifting condensation level, and the pressure fields.

The trade winds are far from the constant speed, constant direction winds implied by their name. Almost by definition, the name implies an equatorward component of the flow, except when they cross the equator because of the seasonal displacement of the intertropical convergence zone.

For the purposes of this model, the trade winds need not blow toward the equator. For this model, they have been defined, tentatively, to be those winds between 20° N and 20° S and those winds between 20° N and 30° N, or between 20° S and 30° S, that have a component toward the equator. The trades according to this definition will extend from the equator to the axis of the subtropical highs and farther poleward on the eastern sides of the highs. At 30° N or S, the Cardone model should in principal do as well as the trade wind model to be given below.

---

*
See references.

The trade winds are described by a two layer model. The first layer is a constant flux layer with a logarithmic wind profile below the height, z = H. The second layer describes a constant vector wind above H to an elevation of several hundred meters. In the constant vector wind layer, the pressure gradient force is balanced by the coriolis force and the constant rate of decrease of eddy momentum with height above H.

Inputs to the model are the pressure field, the height of the lifting condensation level and cloud activity data. The output is the wind speed and direction at any height between the surface and several hundred meters. The model yields continuously varying wind fields at the equator because the wind stress on the sea surface provides the required balance when the coriolis force vanishes.

The height, h, at which the internal boundary condition is satisfied in the Cardone model, is quite high in the tropical regions because the coriolis force becomes small and because the geostrophic wind level for the Ekman spiral increases as one approaches the equator. For these reasons, the previous model is not a good model for the tropics.

A requirement of any alias removal algorithm to be used with SEASAT and of any techniques developed to compare the surface winds obtained by SEASAT with meteorological winds is that the meteorological winds must be described from conventionally obtained data sources and must not depend as a first go around on any information obtained by SEASAT. The concept is to feed back the SEASAT data into the meteorological analysis so as to improve it. If the vector winds, after being dealiased are recycled through the meteorological thoery, the result should be an improved initial value specification of the appropriate meteorological fields for numerical weather prediction.

The wind fields in the tropics near the surface of the ocean are very complex. Streamline and isotach analyses of these wind fields yield complicated regions of convergence and divergence and singular points where the air is believed to stagnate along lines of inflow and outflow.

The results of this analysis are that knowledge of the lifting condensation level will be needed for the Fleet Numerical Weather Central as an additional input field to TWINDX, and that the knowledge of the pressure field will be essential in determing the vector wind in the trade wind regions. Accurate knowledge of the pressure field in the tropics may not actually be available, but the approach given in this paper seems to be the best one possible at the present time. It is capable of numerous extensions that will be described at the end of this paper.

Also needed, but not readily available, is the momentum flux through the lifting condensation level. Further study of this flux in terms of cloud activity may make it possible to allow this flux to vary. Present data suggest that it can range from zero to 10% of the momentum flux near the sea surface.

7.2 Governing Equations of Motion

The governing equations of motion for the Trade Winds are equations (132) and (133). They represent the horizontal balance of forces near the surface of the earth. The terms involved are the total change of wind speed with time, the coriolis effect, the pressure gradient and the rate of change with height of the Reynolds stress fluctuations denoted by $< u' \, w' >$ and $< v' \, w' >$.

$$\frac{d\bar{u}}{dt} - f\bar{v} = -\frac{1}{\rho} \frac{\partial p}{\partial x} - \frac{\partial}{\partial z} < u' \, w' > \quad (132)$$

- 55 -

$$\frac{d\overline{v}}{dt} + f\overline{u} = -\frac{1}{\rho}\frac{\partial p}{\partial y} - \frac{\partial}{\partial z}<v'\,w'> \qquad (133)$$

For this study, the total change with time of u and v will be neg-
lected. It would be possible to account for the nonlinear field accel-
eration terms in a way similar to the way the gradient wind is calculated
from the geostrophic wind, if this level of sophistication is required.
If this were done, only the local change with time of the wind would be
neglected. For purposes of analysis, this assumption is a perfectly
justifiable one because it is found that the remaining terms do indeed
balance to within a few percent at a particular observation time.

The next step is to rotate the x,y coordinate system to a local
coordinate system in such a way that $\overline{v}$ and $<v'\,w'>$ are both zero.
That is the Reynolds stress in one particular direction, and the wind
speed in that direction are both zero. Under these assumptions equa-
tions (132) and (133) become equations (134) and (135).

$$0 = -\frac{1}{\rho}\frac{\partial p}{\partial x} - \frac{\partial}{\partial z}<u'\,w'> \qquad (134)$$

$$f\overline{u} = -\frac{1}{\rho}\frac{\partial p}{\partial y} \qquad (135)$$

7.3 Data on $\overline{u}(z)$ and $<u'\,w'>$

Data for five trade wind regimes for varying levels of cloud
activity have been tabulated in the report of the U.S. Gate Central
Program Workshop, (Greenfield et al. (1977)). Graphs of the wind
speed as a function of height on a logarithmic height scale, of the
wind speed ± one standard deviation, and tabulated values of the wind
direction ± one standard deviation are given on each of the next five

figures. Figure 7 is catagorized as corresponding to stationary cloud conditions where the clouds are neither increasing nor decreasing. Figure 8 is catagorized by the condition that the clouds are growing. Figure 9 is catagorized by the condition that the clouds are decaying. Figure 10 is for data that were obtained after a disturbance has passed and describes the effects of the wake of this disturbance. Figure 11 describes stationary conditions once again, except that there is moderate convective activity.

For all of the figures, at the first two points plotted, which correspond to elevations above the sea surface of about 8.7 and 26 meters, there is evidence that a logarithmic wind profile exists. The data are not complete enough to make it possible to determine whether or not the added effects of stability should modify the logarithmic profile somewhat. Above these first two points there is a layer where the wind is essentially constant in speed. As plotted, the circled points describe a reasonable approximation to the upper range of this layer. The standard deviations of the wind speed indicated by the small ticks to each side certainly do not invalidate the hypothesis that the wind is essentially constant over a fairly deep atmospheric layer above the logarithmic wind profile. Above some elevation, roughly 150 or 200 meters, the wind starts to decrease for some of the plots and for others it increases, depending upon the cloud activity. The wind directions for each elevation are shown on the right hand side of each figure. For the very large standard deviations that are indicated (the various means are based on approximately fifteen values), the average wind direction is sensibly constant throughout the entire layer varying by no more than ± 10 or 15 degrees.
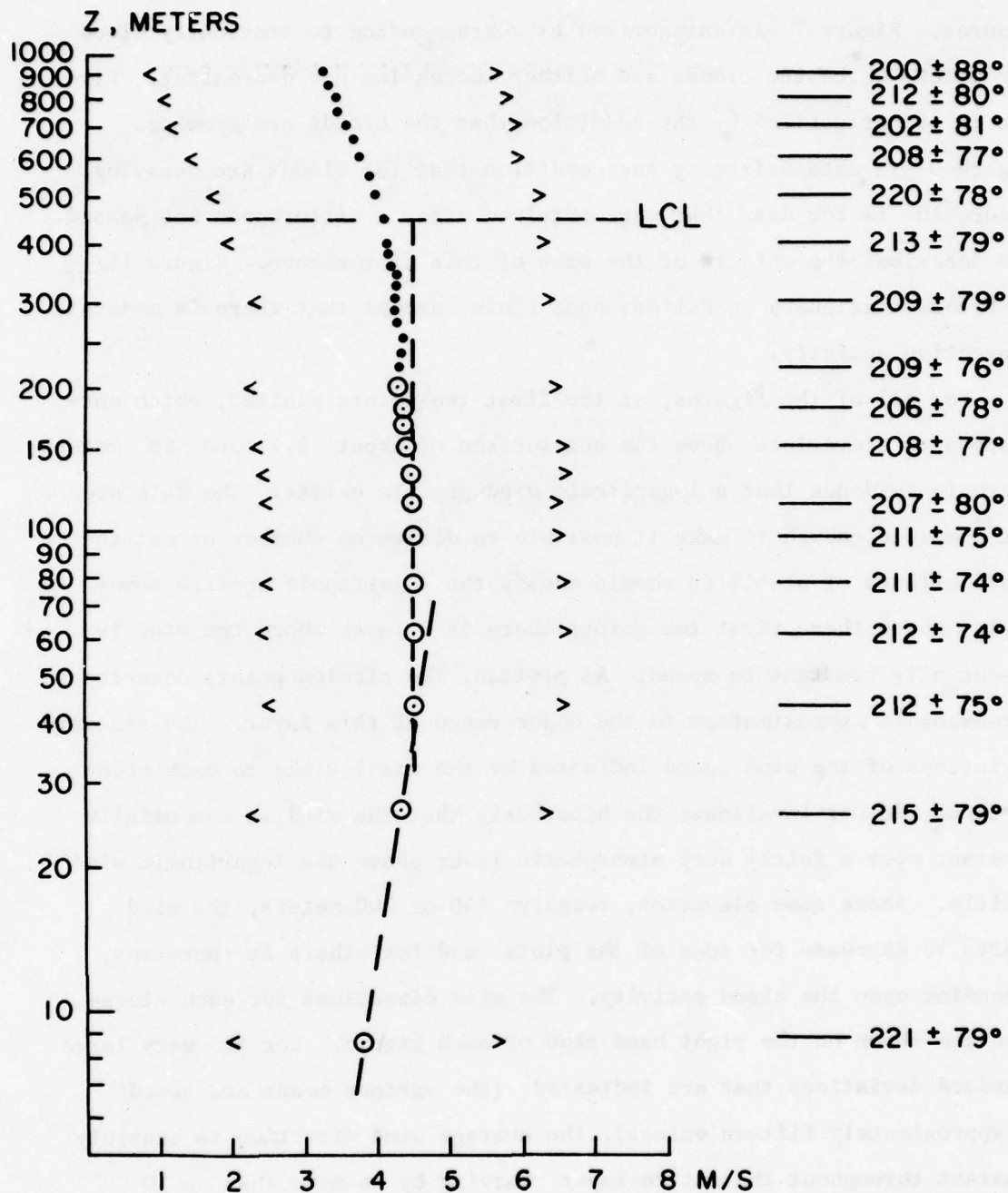
Figure 7. Average wind speed in m/s (± 1 std dev) and
direction (± 1 std dev) in gate area as a function of
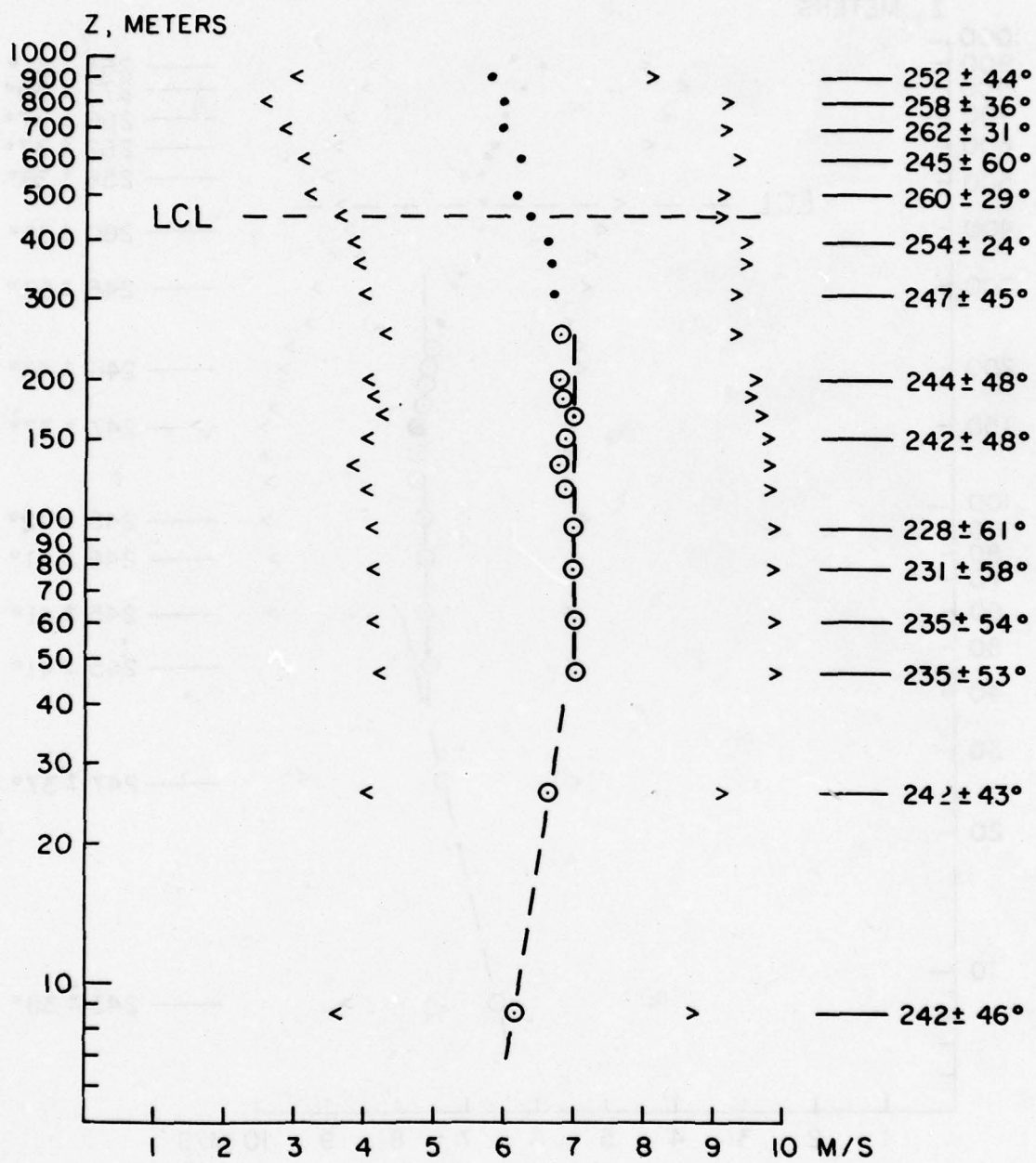elevation during stationary conditions.

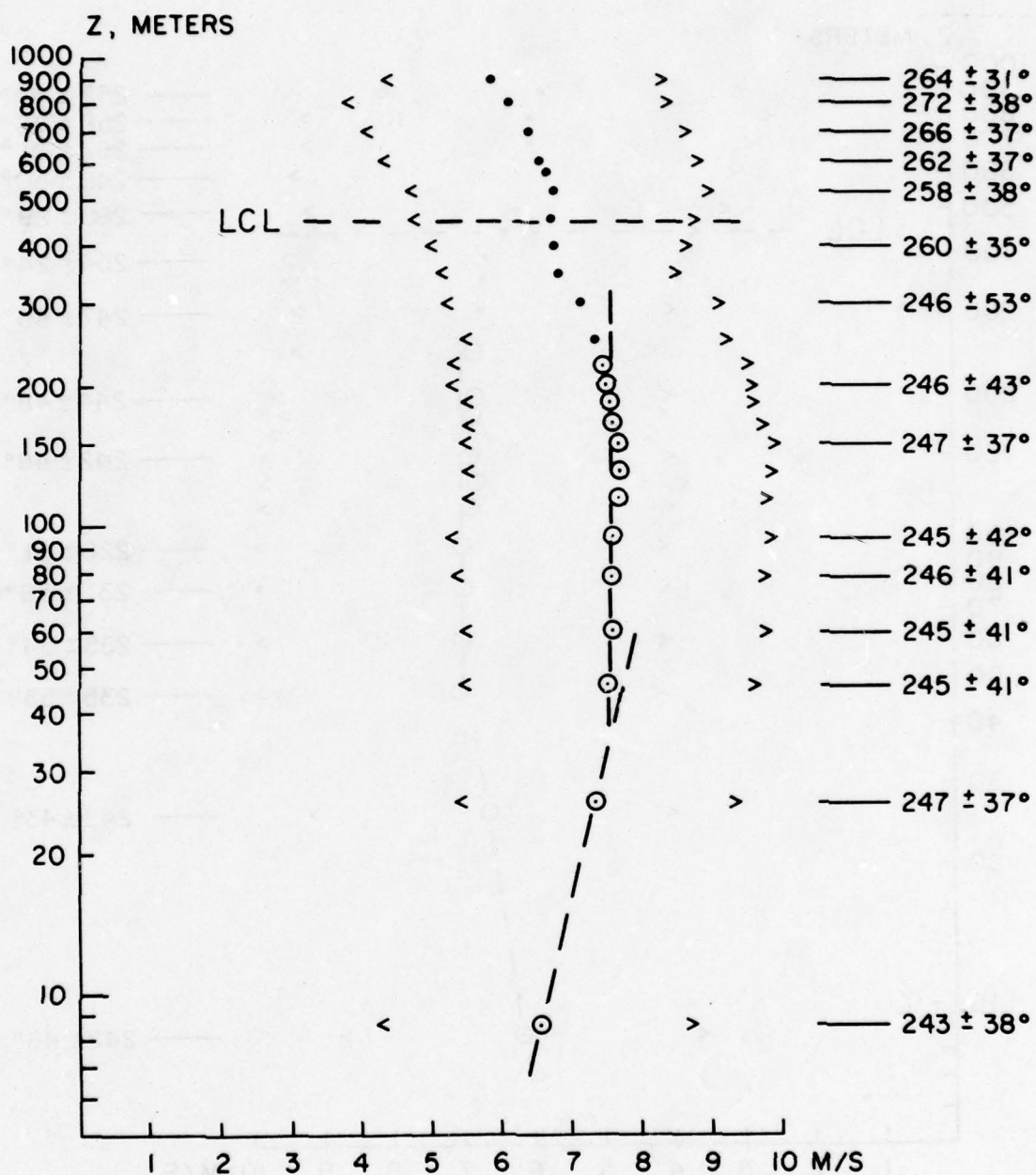Figure 8. Same as Fig. 7 except during growth conditions.

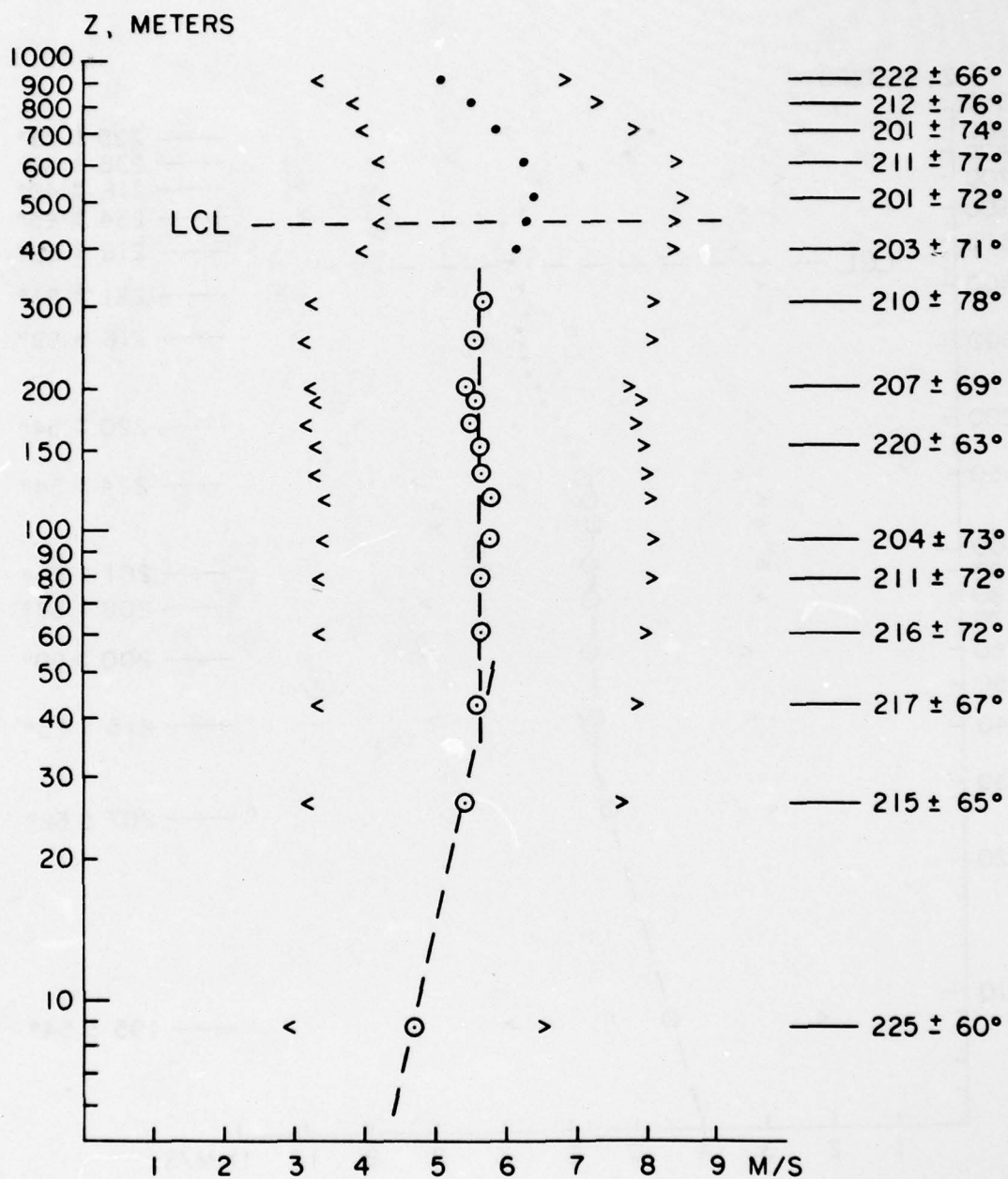Figure 9. Same as Fig. 7 except during decay conditions.

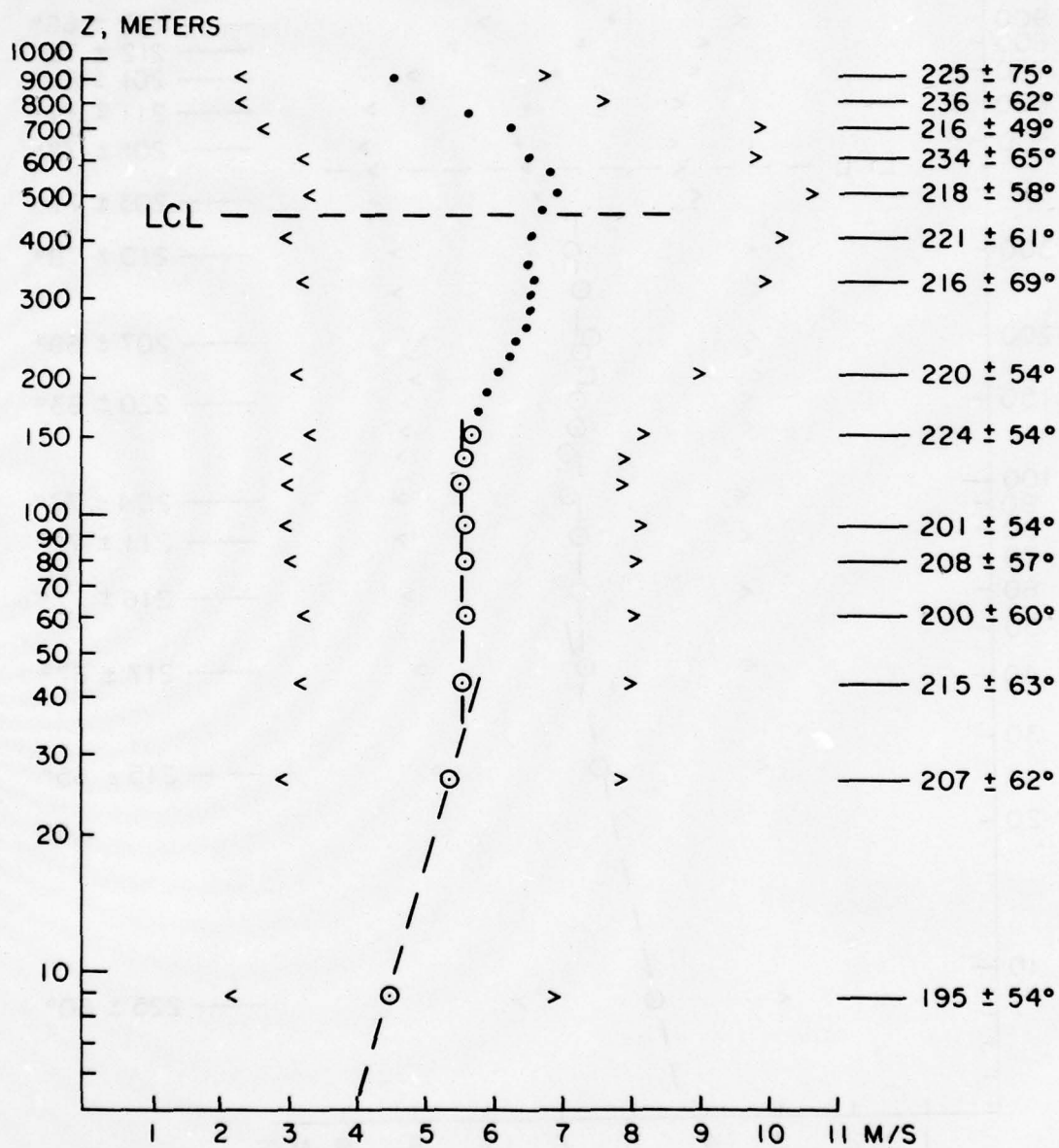Figure 10. Same as Fig. 7 except for wake conditions.

Figure 11. Same as Fig. 7 except for stationary conditions with moderate convection.

The measurement of the average wind conditions and the various fluxes involved in the study of the trade winds appear to be having the same kinds of difficulties that occurred with the aircraft measurements of radar backscatter as discussed in Part 1 of this report. The microscale fluctuations are of a nature such that they interact with the mesoscale features of the cloud dynamics in such a way that it is difficult to obtain stable averages. In a similar way, the aircraft measurements of backscatter could not avoid the kind of fluctuations that were produced by the microscale fluctuations in the wind so that the backscatter measurements from the aircraft were much more unstable than the backscatter measurements to be expected from SEASAT. It should also be mentioned that the fifteen values that were averaged in order to obtain the averages were undoubtedly not independent, so that these standard deviations are based on very small samples.

Nevertheless, the data show that there is a layer near the sea surface where the wind profile is logarithmic and that immediately above it for one hundred or more meters the average wind speed is constant in speed and direction with height. As the trade wind boundary layer approaches the base of the cumulus at the lifting condensation level, which was at approximately 450 meters for this series of observations, deviations from a simple constant vector wind with height become important. Also, the actual wind is very turbulent with large fluctuations around the average value. These features of the trade wind regime need to be modeled in terms of cloud physics. For SEASAT, it is only necessary to describe the synoptic scale average vector wind from the sea surface to some height below the lifting condensation level.

Table 1 summarizes some of the parameters that can be extracted from Figures 7 through 11. The top of the logarithmic profile determined from the intersection of the line representing the region of constant wind with height and the line connecting the two lowest points in the wind profile is given in the first row of the table. For four of the five graphs, the top of the logarithmic profile turns out to be at about 35 meters; for the other one it is closer to 47 meters. For this first effort, the top of the logarithmic profile will be set at 35 meters. An extension to other areas of the trade winds may make it necessary to parameterize the top of the logarithmic profile as some fraction of the height of the lifting condensation level.

Table 1 Parameters of the Trade Winds in BOMEX for Five Different Cloud Conditions.

	Stationary	Growth	Decay	Wake	Stationary with Moderate Convection
Top of Log Profile (m)	35	47	35	35	35
Top of Constant $\bar{U}$ (m)	200	250	220	300	150
$\bar{U}$ (m/s)	4.5	7.0	7.6	5.6	5.5

The top of the layer of constant wind varies from 150 meters in Figure 11 to 300 meters in Figure 10. The determination of the top of this layer is somewhat subjective. It surely extends to at least 100 meters in all of the figures, and for several of them it undoubtedly exceeds 200 meters. The model to be derived will thus attempt to describe the wind from the surface of the ocean to a height of at least 100 meters (and perhaps much higher) in the tropical regions of the world oceans.

The motions of cumulus clouds in the tropics obtained from successive images generated by a geostationary satellite are being used to estimate the winds over the ocean both at the cloud base and nearer to the sea surface. Hasler et al. (1977) made aircraft measurements in the Caribbean and the Gulf of Mexico of wind speed and direction at 150 meters and at the cloud base and compared them with cloud motions. The cloud speeds varied from 12.5 to 5.1 m/s during the experiment. The magnitude of the vector difference between the cloud motion and the wind at the cloud base was 1.5 m/s. The magnitude of the vector difference between the cloud motion and the wind at 150 m was also 1.5 m/s. Direction differences, per se, were below the accuracy of the measurement system, as were any systematic biases. The surface winds were thus equally likely to be somewhat stronger or weaker than those found from the cloud motion.

From Figures 7 to 11, a one to one correspondence between the winds either at the cloud base or at 150 m, and the cloud motion should not be expected. The SEASAT SASS winds may make it possible to study these differences on a large scale systematic basis. In particular, clouds can form on either the upwind or downwind side and dissipate on the opposite side depending on features of the atmosphere in which they form. Certain features of the model being derived are intriguing as possible descriptors of the interaction of the field of motion and clouds.

Hubert and Timchalk (1972) compared cloud motions with the winds at the cloud base, cloud middle and cloud top. The best correlation was for winds at the cloud base. Vector errors in which cloud motions were compared with rawinsonde data were 3.5 to 4 m/s, and the mean direction errors were close to 20°. Suggestions were made about techniques for testing whether or not the clouds actually were tracers of the mean wind.

LeMone and Pennell (1976) and Pennell and LeMone (1974) have documented numerous features of the trade wind region. For example, the virtual potential temperature is constant to the base of the clouds, the mixing ratio varies linearly with elevation above the sea surface, and the wind profile with height has features similar to those found for the BOMEX data, except perhaps that the height at which the logarithmic profile begins may be greater in their data. The important feature of these two studies is that they show that the momentum flux decreases from the surface to the cloud base, which can be parameterized as the height of the lifting condensation level for numerical analysis purposes. Other important features of the data presented in these two studies are the standard deviations of the measured winds and the variation of these quantities with elevation. The standard deviations for the winds shown in Pennell and LeMone (1974) are comparable to the standard deviations shown in Figures 7 through 11, if they are combined to represent the standard deviation of the magnitude of the wind and not the standard deviations in the mean direction and the cross wind direction.

The profiles for the momentum flux given in Figure 6 of Pennell and LeMone (1974) and in Figure 5 of LeMone and Pennell (1976) both show a decrease in the momentum flux with elevation to a value that is nearly but not exactly, zero at the cloud base (except for their case 3 of the 1976 study.)

A constant flux layer is suggested by these graphs, but not conclusively demonstrated. The most convincing argument for a constant flux layer would be Figures 7 through 11 of this paper which definitely show a logarithmic variation of the wind with height at the lower elevations, as discussed previously. On the basis of Figures 7 through 11, and on the basis of the argument that the wind must decrease to zero at the sea surface as a boundary condition, a constant flux layer below some level, H, will be used.

7.4 A Two Layer Model

The problem of describing the winds in the trade wind regions of the earth from the surface to 150 or 200 meters above the surface thus becomes a two-layer problem. For the region from the surface to the level, H, as defined by equation (136) the assumption of a constant momentum flux must be made as shown in Figure 12. Under this assumption, equation (134) and (135) above become equation (137). The dominant feature of the wind in this surface layer must be the fact that the rate of change with height of the momentum flux is identically zero. This leads to the definition of the friction velocity as given by equation (138).

$$0 \leq z \leq H \tag{136}$$

$$\frac{\partial}{\partial z} < u' w' > = 0 \tag{137}$$

$$- < u' w' > = u_*^2 \tag{138}$$

If the atmosphere is neutrally stratified, then it follows that the wind in this layer is defined by equation (139).

$$\bar{u} = \frac{u_*}{\kappa} \ln (z/z_o) \tag{139}$$

These equations simply state that the layer above of constant speed and direction of the wind for this layer.

The layer above H is modeled by the requirement that the rate of change with height of the momentum flux is constant as stated by equation (140).

$$- \frac{\partial}{\partial z} < u' w' > = \text{constant} \tag{140}$$

- 67 -

The description of the momentum flux as a function of height is given by Figure 11. At the level, H, the momentum flux must equal the value at the surface. This is indicated by equation (141). At the lifting condensation level, h_{LCL}, there will be a residual momentum flux that is some fraction (R) of the momentum flux at H. This is indicated by equation (142).

$$\text{At } H, \qquad\qquad - < u' w' > = u_*^2 \qquad\qquad (141)$$

$$\text{At } h_{LCL}, \qquad\qquad - < u' w' > = R u_*^2 \qquad\qquad (142)$$

For the region, $H \leq z \leq h_{LCL}$, the equation for the momentum flux is then given by equation (143), as illustrated in Figure 12

$$- < u' w' > = u_*^2 - \frac{(u_*^2 - R u_*^2)}{h_{LCL} - H} (z-H) \qquad\qquad (143)$$

Its derivative by the very nature by which it was constructed is then equation (144).

$$\frac{\partial}{\partial z} < u' w' > = u_*^2 (1-R)/(h_{LCL} - H) \qquad\qquad (144)$$

Under these conditions, (134) and (135) now become equations (145) and (146).

$$0 = - \frac{1}{\rho} \frac{\partial p}{\partial x} - \frac{(1-R) u_*^2}{(h_{LCL} - H)} \qquad\qquad (145)$$

$$\bar{f u} = - \frac{1}{\rho} \frac{\partial p}{\partial y} \qquad\qquad (146)$$
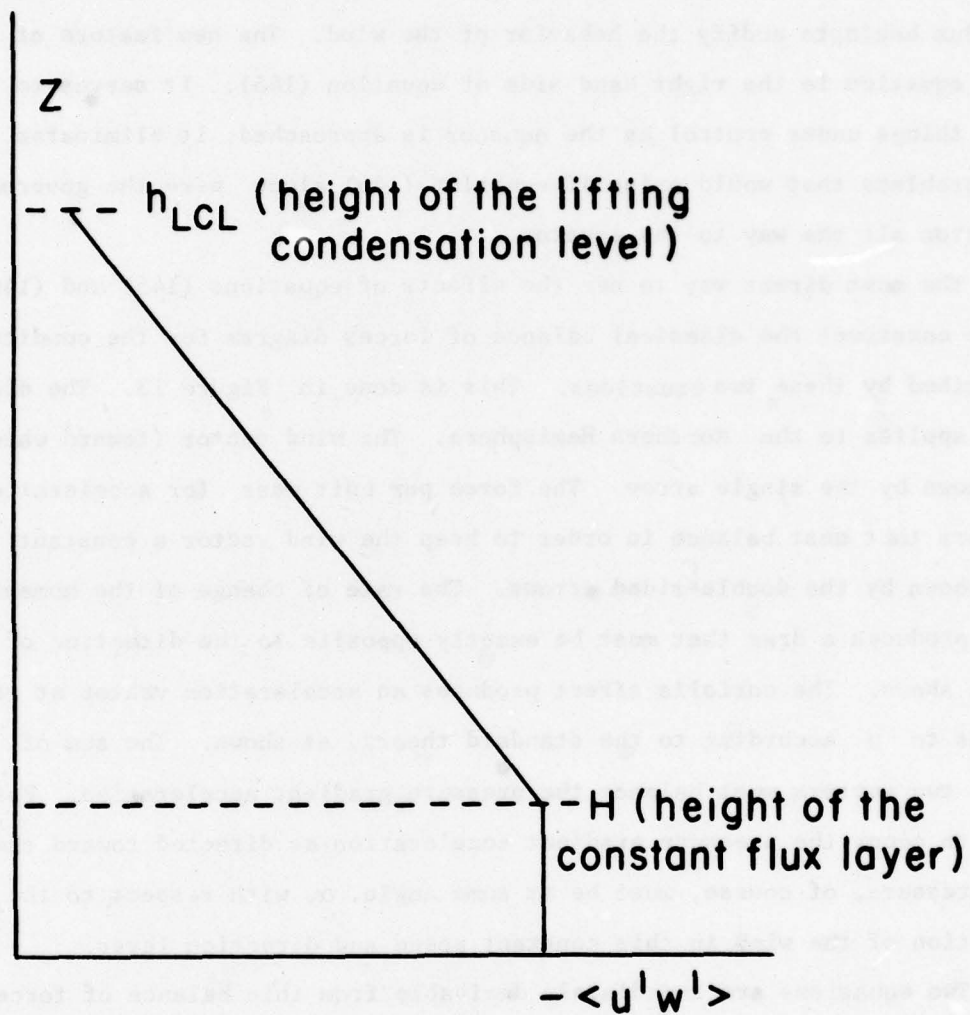
- 68 -

Figure 12. Momentum flux as a function of height in the trade winds.

Since these equations are not a function of height, they describe
a wind independent of height in the layer immediately above the height,
H, up to a height where the turbulent effects from the activity of the
cumulus begin to modify the behavior of the wind. The new feature of
this equation is the right hand side of equation (145). It serves to
keep things under control as the equator is approached; it eliminates
the problems that would arise if equation (146) alone were the governing
equation all the way to the equator.

The most direct way to see the effects of equations (145) and (146)
is to construct the classical balance of forces diagram for the conditions
described by these two equations. This is done in Figure 13. The dia-
gram applies to the Northern Hemisphere. The wind vector (toward which)
is shown by the single arrow. The force per unit mass (or acceleration)
vectors that must balance in order to keep the wind vector a constant
are shown by the double-sided arrows. The rate of change of the momentum
flux produces a drag that must be exactly opposite to the direction of
u as shown. The coriolis effect produces an acceleration vector at right
angles to u according to the standard theory, as shown. The sum of
these two vectors must balance the pressure gradient acceleration. For
this to occur the pressure gradient acceleration as directed toward the
low pressure, of course, must be at some angle, α, with respect to the
direction of the wind in this constant speed and direction layer.

Two equations are immediately derivable from this balance of forces
diagram. The first simple states that the sum of the squares of the two
forces that oppose the wind, must balance the square of the force that
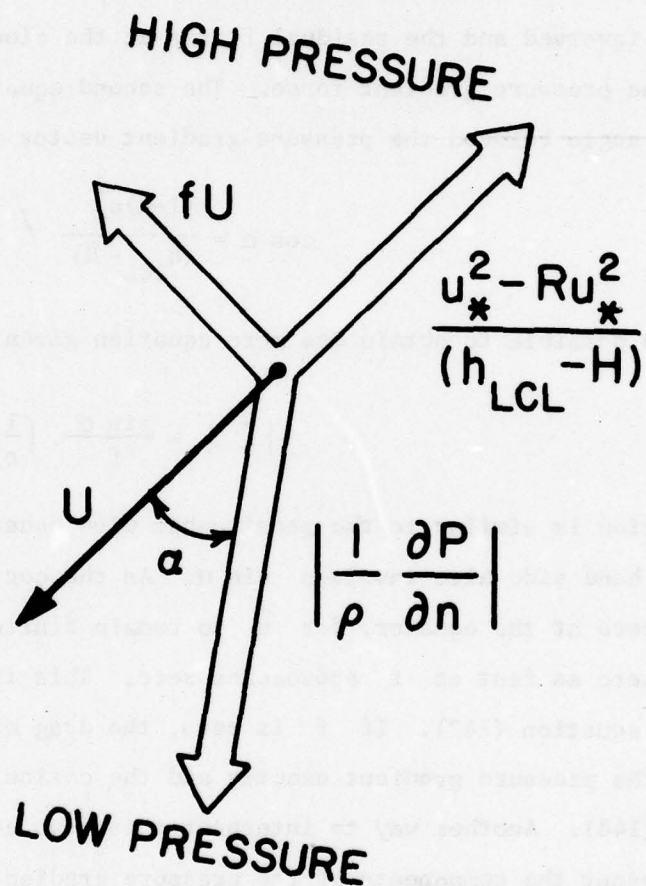accelerates the wind, and this is equation (147).

- 70 -

Figure 13. Balance of forces diagram for the trade winds.

$$(f\bar{u})^2 + \left(\frac{1-R}{h_{LCL}-H}\right)^2 u_*^4 = \left| \frac{1}{\rho} \frac{\partial p}{\partial n} \right|^2 \qquad (147)$$

As written, it requires a knowledge of the wind speed at some height above H, and of the wind stress at the sea surface as well as the thickness of the layer involved and the residual fluxes at the cloud base. These must balance the pressure gradient force. The second equation, (equation 148), given the angle between the pressure gradient vector and the vector wind.

$$\cos \alpha = \frac{(1-R)u_*^2}{(h_{LCL}-H)} \Bigg/ \left| \frac{1}{\rho} \frac{\partial p}{\partial n} \right| \qquad (148)$$

It is also possible to obtain one more equation given by equation (149).

$$\left| \bar{u} \right| = \frac{\sin \alpha}{f} \left| \frac{1}{\rho} \frac{\partial p}{\partial n} \right| \qquad (149)$$

This equation is similar to the geostrophic wind equation except that the right hand side also involves $\sin \alpha$. As the coriolis force approaches zero at the equator, for $\bar{u}$ to remain finite, $\sin \alpha$ must approach zero as fast as f approaches zero. This is even more clearly stated in equation (147). If f is zero, the drag of the wind stress balances the pressure gradient exactly and the cosine of α is one in equation (148). Another way to interpret these two equations is that they represent the components of the pressure gradient force parallel to and normal to the wind vector.

At the height, H, the wind must be continuous. The value obtained from equation (139), with $z = H$, must correspond to the value for the wind given in equation (147).

If the pressure gradient, the height of the lifting condensation level and the value of R are known, and if equation (139) and (147) are used, there are three unknowns, in a sense, at this stage of the analysis. They are the wind speed, the value of u_* and the value of z_o. It can be assumed that the value of R can be parameterized, perhaps on the basis of cloud cover and cloud changes, that the height of the lifting condensation level can be determined from surface measurements by ships, and that the height H is either a constant (equal to 35 meters) as the data seem to indicate, or some fraction of the height of the lifting condensation level.

The problem can be closed by assuming a relationship between z_o and u_*. If this is done, then the wind speed at the height H is a function of the friction velocity, and equation (147) can be written entirely in terms of the friction velocity and known parameters for the *left hand side and the pressure* gradient on the right hand side.

For this particular application, the relationship that has to be assumed between the friction velocity and the roughness length will be critical because, as can be seen, equation (16) depends on the fourth power of the friction velocity. If equation (62c) is combined with equation (139) and if the result is substituted into equation (147), the result is equation (150).

$$\left(\frac{fu_*}{\kappa} \ln\left(\frac{H}{z_o}\right)\right)^2 + \left(\frac{1-R}{h_{LCL}-H}\right)^2 u_*^4 = \left|\frac{1}{\rho}\frac{\partial p}{\partial n}\right|^2 \tag{150}$$

From the data available to the Fleet Numerical Weather Central on the height of the lifting condensation level and on the pressure field in the tropics, the problem is now essentially solved. Reasonable values for R can be tried and reasonable values for H, so that the left hand side of equation (20) is entirely a function of u_*. At a given point on the Fleet Numerical Weather Central 123 x 123 polar sterographic grid, the term on the right hand side can be found. Values of u_* can be substituted into the left hand side until the equation balances. It is probably not necessary to attempt to solve this problem analytically especially since the first term involves a very complicated function of u_* in the denominator of the natural logarithm. A first approximation for u_* would be to set f equal to zero and solve equation (150). This would provide an upper bound for u_*. Lower values successively searched would then yield the value of u_* that satisfies the equation.

Once the value of u_* is known, the magnitude of the wind at the height, H, can be computed from equation (151). (In fact, in a computer program it would be known in the process of solving equation (150)).

$$\bar{u}(H) = \frac{u_*}{\kappa} \ell n \ (H/z_o) \qquad (151)$$

Finally the angle, α, can be found from equation (148). Thus the wind speed and direction at the height, H, are known. This wind speed and direction would be measured at any height above H for a thickness of perhaps several hundred meters.

The measurements by which backscatter has been related to wind speed have been related to a wind measured at 19.5 meters. Since u_* is

- 74 -

known this wind can be calculated from equation (152). It will be some-
what less than the wind speed at the height, H.

$$\bar{u}(19.5) = \frac{u_*}{\kappa} \ell n \, (1950/z_o) \tag{152}$$

In TWINDX, the value of u_* is found by rewriting equation (150)
as equation (153), A first guess for u_* is found by solving (150) with
f = 0. This yields an upper bound for u_*. A lower bound is zero. A
new trial value for u_* half way between the two bounds is found and sub-
stituted into the right hand side of (153). If this right hand side is
greater than one, the new value of u_* becomes the new upper bound. If
it is less than one, the value of u_* becomes a lower bound. Half the
distance between these new bounds then generates a new trial value for
u_*, which is again tested and becomes a candidate for either a new upper
or lower bound. The process is continued until the trial value of u_*
yields a left hand side for (153) that differs from one by 0.0001.
This value of u_* is then used to find α, $\bar{u}(35)$ and $\bar{u}(19.5)$.

$$\frac{\left(f \ell n \left(H/z_o \right) / \kappa \right)^2 u_*^2}{|\frac{1}{\rho} \frac{\partial p}{\partial n}|^2} + \frac{\left(1-R \right)^2 u_*^4}{\left(h_{LCL} - H \right)^2 |\frac{1}{\rho} \frac{\partial p}{\partial n}|^2} = 1 \tag{153}$$

Provision has been made in TWINDX for an input field for h_{LCL},
H has been assumed to be 35 m, and R has been assumed to be zero.

If CP (for cloud physics) is defined to be equation (154),

$$CP = \frac{1 - R}{h_{LCL} - H}$$

(154)

the factor that multiplies u_*^2 in (143), (144), (145) and (148) can be expressed as a field variable on a polar stereographic grid and used to replace the field for h_{LCL}. Modifications of subroutine TRADES by changing several lines of code, would then allow the use of the CP field instead of the h_{LCL} field. This field could then be prepared by some other program for use by TWINDX.

7.5 Degrees of Improvement

The model described herein can be applied with increasing sophistication as various improvements are made. Given the height of the lifting condensation level, and the pressure field in the tropics, a first approximation would be to set $R = 0$ and $H = 35$ m as in TWINDX, and assume neutral atmospheric stability. It would also be possible to try the assumption that the height H is some fraction of the height of the lifting condensation level.

As another improvement for this model, the air-sea temperature difference would be required which provides some information on atmospheric stability. It would then be possible to replace the logarithmic wind profile below H by the Monin-Obukhoff profile, which can be expressed in terms of the air-sea temperature difference and the other quantities. The major change would be in the definition of the wind speed, $\bar{u}$, for

the left hand side of equation (20). This would require a second term to describe the fact that the Monin-Obukhoff profile departs from the logarithmic wind profile by the time the height, H, is reached. The rest of the derivation remain essentially unaltered.

A third improvement would result from attempts to estimate the quantity R as a function of the cloud cover in the area of interest and whether or not the cumulus clouds were building or decaying because of effects at and near the lifting condensation level. This would take care of the residual fluxes through the lifting condensation level caused by vertical and horizontal motions induced by the cloud cover. This particular approach could perhaps at a future time be merged with other data to obtain R and H so as to generate the quantity, CP. It is not anticipated that the value of R would be much more than about 0.1.

7.6 The Interaction of Clouds and Winds

The trade wind model has features that relate cloud behavior and winds near the surface of the ocean. For the first time, the accuracy of SEASAT winds may be sufficient to detect some of these features.

As an oversimplified example , consider motion on a plane earth near 10° N where the coriolis term is 2.5×10^{-5}, and a zonally symmetric wind field containing an east-west oriented band of clouds as in Figure 14. The isobars (not shown) run east-west also. The friction velocity north and south of the cloud band is assumed to be 30 cm/sec. With h_{LCL} = 450 m, H = 35 m, and R = 0, enough has been assumed to permi the calculation of the pressure gradient acceleration which equals 3.16×10^{-2} cm/sec^2. The wind above H is from 46.74° and has a speed of 9.34 m/s.

At the center of the cloud band, let R = 0.1, and let the other parameters be unchanged. Then the friction velocity must increase to 31.05 cm/sec. The wind above H is from 48.76^o and the speed is 9.62 m/s. The component inside the band that is parallel to the wind outside the band is 9.61 m/s and the component normal to it is 0.34 m/s. The continuity equation then suggests that there will be convergence north of the center of the band and divergence south of it.

The conditions are illustrated from another point of view in the north south section through the cloud band shown in the bottom half of the figure. For a steady state, the convergence in the lower level winds upwind could cause new clouds to form at the upwind edge of the band. They would travel southwestward through the band and dissipate at the southern edge because of the divergence in the lower level winds. Slight imbalances with stronger convergence upwind shifted northward and divergence downwind shifted northward could cause the band to migrate northward (analogous to group velocity effects in capillary waves) and conversly with convergence shifted southward, the band would migrate southward. The cloud band can move with a speed and direction that is much different from the speeds and directions of the clouds within it. The formation, shape, speed and direction and dissipation of a band of clouds is not the same as the formation, speed, direction and dissipation of an individual cloud in that band. A combination of SEASAT data and cloud motion studies should make it possible to unravel some of these effects.

If wave-like undulations in the lifting condensation level due to variations in water vapor content have a greater effect than variations in R, a lowered h_{LCL} band, or zone, of lifting condensation level
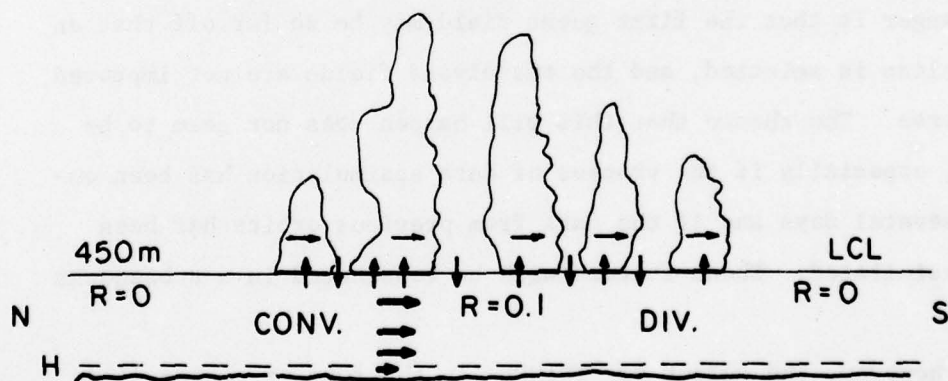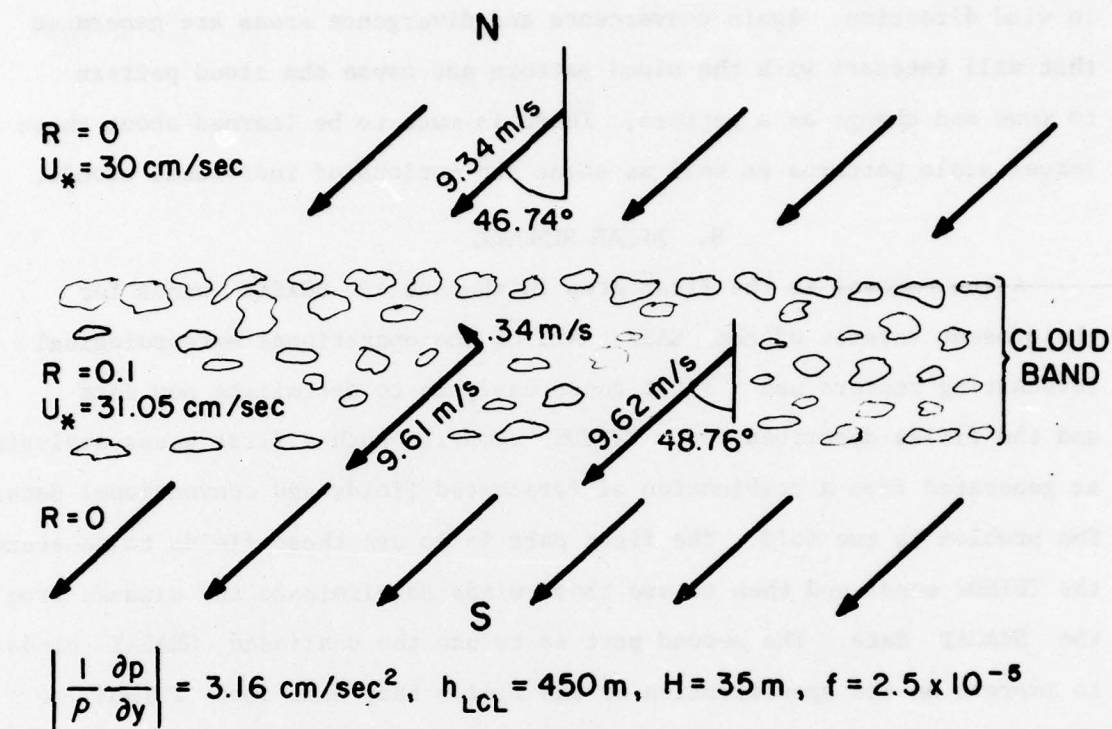
- 78 -

Figure 14. Schematic example of the interaction
of clouds and winds.

heights causes a decrease in the wind speed and a counterclockwise change
in wind direction. Again convergence and divergence areas are generated
that will interact with the cloud pattern and cause the cloud pattern
to move and change as a pattern. There is much to be learned about these
larger scale patterns as well as about the motions of individual clouds.

8.   ALIAS REMOVAL

Alias removal is the first step in the use of SEASAT winds for
the present version of the SASS. All of the operational meteorological
forecasting centers use a first guess analysis to assimilate new data
and the fields described for   TWINDX   comprise such a first guess analysis
as generated from a combination of forecasted fields and conventional data.
The problem is two fold. The first part is to use these fields to generate
the TWINDX winds and then to use these winds to eliminate the aliases from
the SEASAT data. The second part is to use the dealiased SEASAT winds
to improve on the specification of the fields that went into TWINDX so
that these improved fields can then be used for improved forecasts.

The danger is that the first guess field may be so far off that an
incorrect alias is selected, and the reanalysed fields are not improved,
but made worse. The chance that this will happen does not seem to be
very large, especially if the process of data assimulation has been on-
going for several days and if the data from previous orbits has been
properly assimilated. These factors will be considered in a subsequent
report.

Given however, the output of TWINDX in the form of vector winds
corrected to a neutrally stratified atmosphere for h and h + 3 where
h is 0, 3, 6, 12, 15, 18, or 21 hours, and a SEASAT pass starting at

h + Δt (where $0 < \Delta t < 3$) from the equator to landfall, (or landfall to the equator), the first step is to eliminate the aliases in the SASS winds. The time of the pass should be adjusted to correspond to the most actively changing portion of the wind field so that a reference time would be $h + \Delta t + \Delta t' = h + \Delta t^*$.

if $\vec{V}_h$ is the TWINDX wind at h and $\vec{V}_{h+3}$ is the wind at h+3, let

$$\vec{V}_m = \vec{V}_h + \Delta t^* \, (\vec{V}_{h+3} - \vec{V}_h)/3 \tag{154}$$

for each point of the 123 x 123 grid. Finer interpolation to any latitude and longitude is probably justifiable.

Then let

$$\vec{V}_{R1}(\lambda,\varphi), \vec{V}_{R2}\,(\lambda,\varphi)$$

$$\text{or} \qquad \vec{V}_{R1}(\lambda,\varphi), \vec{V}_{R2}(\lambda,\varphi) \;\; \vec{V}_{R3}\,(\lambda,\varphi)$$

$$\text{or} \qquad \vec{V}_{R1}\,(\lambda,\varphi), \vec{V}_{R2}(\lambda,\varphi), \vec{V}_{R3}\,(\lambda,\varphi), \vec{V}_{R4}(\lambda,\varphi) \tag{155}$$

be the possible solutions for the SASS winds. Then

$$\min(A) = |\, \vec{V}_{RA} - \vec{V}_M \,|^{\,2}, \tag{155}$$

where A varies over 2, 3 or 4 values, yields that SASS wind with the minimum vector difference from the TWINDX wind. This vector wind should be used in subsequent analyses as the true wind. The way in which this SASS wind differs from the TWINDX wind contains information that can be used to correct the initial value analysis fields for either the time, h or the time, h+3.

The subject of the removal of aliases and the use of the SASS
winds so obtained for the improved specification of the initial values
for a numerical weather prediction will be treated in a subsequent
report. The winds near the surface of the ocean contain information
about a thick layer of the atmosphere and it is necessary to be able
to extract this information and apply it correctly to the various levels
and layers of the presently operational primative equation models as
usually given in a σ vertical coordinate system.

9. REFERENCES

Baer, L. (1962): An Experiment in Numerical Forecasting of Deep Water Ocean
Waves. Lockheed Missles and Space Co., Sunnyvale, Calif.

Brown, R. A. (1978): Similarity Parameters from First Order Closure Data
Boundary Layer Meteorology Vol. 14, pp. 381-395.

Brunt, D. (1942): Weather Study. The Roland Press Company; 215 pp.

Brunt, D. (1944): Physical and Dynamical Meteorology, Cambridge University
Press; 428 pp.

Businger, J. A., I.C. Wyngaard, Y. I. Zumi and E. F. Bradley: Flux-profile
relationships in the Atmospheric Surface Layer. J. Atm. Sci., Vol. 28,
pp. 181-189.

Cane, M. A., V. J. Cardone, M. Halem, I. Halberstam and J. Ulrich (1978):
Realistic Simulations of the Global Observing System and of SEASAT-A
Marine Wind Data. NASA/GSFC   Unnumbered Report.

Cardone, V. J. (1969): Specification of the wind field distribution in the
marine boundary layer for wave forecasting. Rep. TR 69-1, Geophys.
Sci. Lab., New York University.

Cardone, V. J., J. D. Young, W. J. Pierson, R. K. Moore, et al. (1976): The
Measurement of the Winds Near the Ocean Surface With a Radiometer-
Scatterometer on Skylab. A Joint Meteorological Oceanographic and
and Sensor Evaluation Program for Experiment S193 on Skylab. NASA
CR-147487.

Charnock, H., (1955): Wind stress on a water surface. Quart. J. Roy. Meteor.
Soc., 81, 639-640.

Dyer, A. J. and B. B. Hicks (1970): Flux-gradient Relationships in the Con-
stand Flux Layer. Quart. J. Roy. Meteor. Soc., Vol. 96, pp. 715-721.

Garratt, J. R. (1977): Review of drag coefficients over oceans and continents. M. Wea. Rev., Vol. 105, No. 7, pp. 915-929.

Greenfield, R. et al. (1977): Report of the U.S. Gate Central Program Workshop NCAR Boulder, Colorado.

Hasler, A. F., W. E. Shenk and W. C. Skillman (1977): Wind Estimates from Cloud Motions: Results from Phases I, II and III of an In Situ Aircraft Verification Experiment. J. App. Meteor., Vol. 16, No. 8, pp. 812-815.

Hubert, L. F. and A. Timchalk (1972): Convective Clouds as Tracers of Air Motion. NOAA TECH MEMO NESS 40.

Johnson, P. W. (1955): The Ratio of the Sea Surface Wind to the Gradient Wind in Johnson, J. W. ed. Proc. First Conf. on Ships and Waves Stevens Inst. of Tech., Hoboken, New Jersey. Oct. 1954 Berkley Council on Wave Research, 509 pp.

Lazanoff, S. M., and N. Stevenson (1975): An Evaluation of a Hemispherical Operational Wave Spectral Model, Tech. Note 75-3, Fleet Numerical Weather Central, Monterey, California.

LeMone, M. A. and W. T. Pennell (1976): The Relationship of Trade Wind Cumulus Distribution to Subcloud Layer Fluxes and Structure. M. Wea. Rev., Vol. 104, No. 5, pp. 524-539.

Melville, W. K., (1977): Wind stress and roughness length over breaking waves. J. Phys. Oceanogr., Vol. 7, No. 5, pp. 702-710.

Meresca, J. (1977): Informal notes on the Planetary Boundary Model of Cardone. NOAA/N.W.S.

Monin, A. S. and A. M. Obukhoff (1953): Dimensionless Characteristics of Turbulence in the Atmospheric Surface Layer. Doklady AN SSSR 93 223-226.

Panofsky, H. A. (1963): Determination of Stress from Wind and Temperature Measurements. Quart. J. Roy. Meteor. Soc., Vol 85, pg. 85.

Panofsky, H. A. and E. L. Peterson (1972): Wind Profiles and Characteristics of Terrain Roughness at Risø. Quart. J. Roy. Meteor. Soc., Vol. 98, pp. 845-854.

Pennell, W. T. and M. A. LeMone (1974): An Experimental Study of the Turbulence Structure in the Fair-Weather Trade Wind Boundary Layer. _J. Atmos. Sci._, Vol. 31, No. 5, pp. 1308-1323.

Petterssen, S. (1940): Weather Analysis and Forecasting, McGraw-Hill Book Company, 505 pp.

Pierson, W. J., (1964): The interpretation of wave spectrums in terms of the wind profile instead of the wind measured at a constant height. _J. Geophys. Res_., Vol. 69, No. 24, pp. 5191-5203.

Pierson, W. J. (1978): Verification Procedures for the SEASAT measurements of the Vector Wind with the SASS. CUNY Institute of Marine and Atmospheric Sciences. Appendix E to Pierson, W. J. and R. E. Salfi (1978): The Theory and Data Base for the CUNY SASS Wind Vector Algorithm. Part 1 of a Final Report submitted to JPL and NEPRF.

Pierson, W. J. and R. E. Salfi (1978): Verification Results for the Spectral Ocean Wave Model (SOWM) by Means of Significant Wave Height Measurements Made by the GEOS-3 Spacecraft NASA CR 60289 Wallops Flight Center Wallops Island, VA.

Salfi, R. E. (1974): Operational Computer Based Spectral Wave Specification and Forecasting Models, prepared for SPOC/NESS/NOAA, CUNY Inst. of Marine and Atmos. Sciences, The City College of the City University of New York.

Tchen, C. M. (1977): Similarity Theory of Surface Boundary Layer _in_ Modern Developments in the Theory of Turbulence (Lecture Notes).

Thomasell, A. and J. G. Welsh (1963): Studies of the Specification of Surface Winds Over the Ocean. The Travelers Research Center, Inc. Final Report on Contract N62306-1025 USNOO.

Wong, V. and T. N. Krishnamurti, (1978): An Algorithm for Removing the Aliased $\vec{u}_*$ Arising from SEASAT Data with a Baroclinic, Non Stationary, Advective, Unstable Planetary Boundary Layer (Informal Notes).

10. SUPPLEMENTARY REFERENCES

Born, G.; J. Wilkerson and D. Lame (1979) (editors) SEASAT Gulf of Alaska
Workshop Report NASA 622-101 (Final version to appear shortly).

Cardone, V. J. (1978): Specification and Prediction of the Vector Wind on
the Continental Shelf of the United States for Application to an Oil
Slick Trajectory Forecast Program. Final Report Contract T-35430
Prepared for the Techniques Development Laboratory Systems Develop-
ment Office, National Weather Service NOAA.

Halberstam, I. (1978): The Marine Surface Layer and Its Relationship to
SEASAT-A Scatterometer Measurements, Manuscript, Jet Propulsion Lab.

Overland, J. E. and S. J. Ghan (1979): A Program Library for Calculation
of Marine Boundary Layer Winds from Grid Point Pressure Fields (METLIB)
PMEL Technical Memo (Draft), Pacific Marine Environmental Lab., Seattle
Washington.

Pierson, W. J. and R. E. Salfi (1978): The Theory and Data Base for the
CUNY SASS Wind Vector Algorithm Part 1 of a Final Report to JPL
and NEPRF, Contracts 954411 and N00014-77-C-0206 (Including Ap-
pendices A through H) CUNY Institute of Marine and Atmospheric
Sciences.

Pierson, W. J. and R. E. Salfi (1979): A Brief Summary of Verification
Results for the Spectral Ocean Wave Model (SOWM) by Means of Wave
Height Measurements Obtained by GEOS-3. J. Geophys. Res. (In Press).

Salfi, R. E. (1978): Program Description for the CUNY SASS Wind Vector
Algorithm (Part 2 of a Final Report for JPL and NEPRF, Contracts 95411
and N00014-77-C-0206). CUNY Institute of Marine and Atmospheric Sciences.

Van Sickle, K. and G. Dome (1978): A Technique for Correcting Scattering
Coefficient Measurements Performed Within a Lossy Atmosphere Remote
Sensing Laboratory, Center for Research, Inc., The University of Kansas,
Lawrence, Kansas, RSL Technical Report RSL TR 350-1.

Pierson, W. J. (1979): A Suggested Technique for the Assimilation of the SASS
Winds from SEASAT Into National Meteorolgical Center Operational Numerical
Weather Prediction Models. CUNY Institute of Marine and Atmospheric Sciences
at The City College. Final Report: Prepared for the Spacecraft Ocean-
ography Group of the National Environmental Satellite Service, National
Oceanic and Atmospheric Administration under Grant #04-6-158-44049 and
Contract 7-35355.